Operator-Based Linearization approach for modeling of reactive flow and transport relevant to CCS

J.D. Kloosterman

MSc thesis Geo-Energy Engineering
November 18, 2022

Operator-Based Linearization approach for modeling of reactive flow and transport relevant to CCS

by

J.D. Kloosterman

to obtain the degree of Master of Science
at the Delft University of Technology,
to be defended publicly on November 18, 2022 at 1:00 PM.

Student number:	4564340	
Project duration:	November 1, 2021 – November 18, 2022	
Thesis committee:	Dr. D.V. Voskov,	TU Delft, supervisor
	Dr. R. Farajzadeh,	TU Delft, co-supervisor
	Dr. J. Snippe	Shell
	Dr. ir. J.C.L Meeussen	TU Delft
	Prof. Dr. Ir. T. Heimovaara	TU Delft

This thesis is confidential and cannot be made public until December 31, 2022.

TU Delft

Abstract

In this work, a novel globally implicit framework for reactive multiphase flow and transport has been implemented using the simulator DARTS and the geochemical package Reaktoro. This framework applies the Operator-Based Linearization (OBL) approach together with a Gibbs Energy Minimization (GEM) scheme to model complex nonlinear reactive transport and flow. Using component- to element-based transport allows for numerically stable equations. This formulation is used to model the dry-out effect and subsequent precipitation of minerals in the near-wellbore region of subsurface aquifers when injecting CO_2. A kinetic rate in combination with Reaktoro equilibrium calculations is implemented to achieve more accurate precipitation results. The kinetic products are not considered inside of Reaktoro and also not as an element. The consistency at the phase transition boundary has been corrected by using a projection of a plane within the hypercube of zero charge balance. Highly sensitive reactions such as pH, require a high resolution to produce physical results. The parameterization grid can be implemented such that some species have a high resolution within a small variation of concentration. Reaktoro is highly accurate for the complex multiphase thermodynamic and chemical equilibrium calculation, but at phase transition boundaries, the equilibration of the state can be nonphysical. The results have been benchmarked against the existing geochemical simulator from Shell, showing that more physics needs to be implemented, but gives an overall accurate result.

Acknowledgement

After six years of studying, my academic journey comes to an end. This could not have been successful without my family, friends, and professors. My family, who have supported, encouraged, and always believed in me with whatever good or bad happened throughout my studies. My friends, who have made every day enjoyable, and for all of the study hours spend. And finally, my professors, who have guided me and taught me everything there is to know.

Without the guidance of Dr. Denis Voskov, this Master's thesis could not have been accomplished. His knowledge of DARTS and coupling geochemical packages proved to be instrumental in solving many issues of the model. Each time we had a meeting, I came out with more ideas to improve the code. Moreover, he has always been patient and understanding. My thanks for the invitation to present my findings in Bergen, which was not only useful but very interesting to participate in.

My thanks go out to Dr. Rouhi Farajzadeh, who always took the time out of his full schedule to help me with any and all chemical problems. His knowledge of MoReS is incredible, helping me to create the benchmarks. Moreover, I would like to thank him for having me as an intern, it was an incredible time at Shell. Finally, having lunch each day was an absolute joy.

Furthermore, Michiel Wapperom has helped me achieve the kinetic equilibrium. Within several weeks, I had a daily meeting to solve the kinetic problems that I was having and I am grateful for the time that he has taken out of his day.

Also, thanks to all the people at Shell who have guided me throughout my internship. It was great to meet all of the teams and interesting to discuss reactive transport and flow and the problems that have been faced there.

Finally, my special thanks to my mother, father, and step-father, who have always helped me in every way possible and have kept me pushing to find solutions no matter how complicated.

J.D. Kloosterman
Delft, November 2022

List of Figures

List of Tables

List of Abbreviations

Symbol / Abbreviation	Description	Unit
A	Area	m^2
A_f	Frequency factor	$\frac{L}{mols}$
BHP	BottomHole Pressure	-
CCUS	Carbon Capture Utilization and Storage	-
c_r	Rock compressibility	bar^{-1}
D_p	Particle diameter	m
DARTS	Delft Advanced Research Terra Simulator	-
E	Elimination matrix	-
EOS	Equation Of State	-
E_a	Activation energy	$\frac{J}{mol}$
F_c	Fractional flow	-
F_{in}	Mass flux in	$\frac{kg}{day}$
F_{out}	Mass flux out	$\frac{kg}{day}$
G	Gibbs free energy	$\frac{kJ}{mol}$
GEM	Gibbs Energy Minimization	-
GIA	Global Implicit Approach	-
g	Gravity	$\frac{m}{s^2}$
II	Injectivity index	-
J	Jacobian	-
K	Permeability	Darcy
K_eq	Equilibrium constant	-
k	Rate constant	s^{-1}
k_{rj}	Relative permeability of phase j	-
LMA	Law of Mass Action	-
M	Mass	kg
N	number of species	-
n	Moles	mol
n_s	Saturation exponent	-
OBL	Operator-Based Linearization	-
P	Pressure	Bar
P_c	Capillary pressure	Pa
PVT	Pressure Volume Temperature	-
Q	Flow rate	$\frac{m^3}{day}$
Q_r	Reaction quotient	-
R	Ideal gas constant	$\frac{J}{Kmol}$
r	Kinetic rate	$\frac{M}{S}$
S	Entropy	$\frac{J}{K}$

Symbol / Abbreviation	Description	Unit
SIA	Sequential Iterative Approach	-
SNIA	Sequential Non-Iterative Approach	-
s_g	Gas saturation	$\frac{m^3}{m^3}$
s_s	Solid saturation	$\frac{m^3}{m^3}$
s_w	Water saturation	$\frac{m^3}{m^3}$
T_c	Transmissibility	$\frac{Dm}{cP}$
t	Time	day
U_t	Total velocity	$\frac{m}{s}$
v_{ir}	Stoichiometric matrix	-
$\mathbf{v}_j$	Phase velocity of phase j	$\frac{m}{s}$
V	Volume	m^3
WAG	Water Alternating Gas	-
x	Distance	m
x_{cj}	Molar fraction of component c in phase j	$\frac{mol}{mol}$
z	Depth	m
z_c	Molar fraction of component c	-
z_e	Molar fraction of element c	-
α	Activity	-
λ	mobility	$\frac{m^3 s}{kg}$
μ	Viscosity	cP
μ_c	Chemical potential	$\frac{J}{mol}$
ν	Phase fraction	-
ρ_T^e	Total element-based density	$\frac{kg}{m^3}$
ρ_j	Phase density of phase j	$\frac{kg}{m^3}$
Φ	Sphericity	-
ϕ	Porosity	-

Contents

1 Introduction

1.1. Problem statement

Studies by the IPCC (Pörtner et al., 2022) have shown that there is a rapidly decreasing time frame to combat anthropogenic climate change and keep the worldwide temperature increase under control. At the current rate of 42 $GtCO_2e$/year of greenhouse gas emissions, there is only a couple of decades left before hitting the critical temperature increase of one-and-a-half degrees (Masson-Delmotte et al., 2018). It is therefore imperative that greenhouse gas emissions need to restrained or that the greenhouse gases are captured before being released. The disadvantage of capturing the CO_2 is that it has to be stored somewhere, whilst being cost-effective. One solution is subsurface storage in reservoirs or aquifers for long-term storage, namely Carbon Capture and Storage (CCS). Worldwide, there is a storage capacity for 100-10000 Gt of CO_2 (Bradshaw et al., 2007), which are situated in depleted hydrocarbon reservoirs and aquifers. As aquifers are extensively large, it is a perfect location for storing a large quantity of CO_2.

1.1.1. Trapping mechanisms

As the reason for injecting CO_2 is the containment of the gas, the trapping mechanisms need to be well understood to avoid risks and to estimate the total containment volume possible. Four main trapping mechanisms are the drivers and each of these trapping mechanisms plays a large role in the sequestration of CO_2.

Trapping mechanism	Time	Area	Description
Structural	Immediate	10-100 km	Buoyancy trapping below seal
Residual	0-1000 years	1000 km	CO_2 remains in pore space
Solubility	100-1000 years	10000 km	CO_2 dissolves in brine and migrates down
Mineral	10's-1000 years	10000 km	CO_2 reacts to form stable minerals

Table 1.1: Different CO_2 trapping mechanisms (Bradshaw et al., 2007)

Table 1.1 shows the four main trapping mechanisms with their respective time frame, area, and short description.

At first, the injected CO_2, which is lighter than the brine, will float on top, against the seal, and propagate outwards. During the slow process of solubility trapping, CO_2 will dissolve in the brine, which makes it heavier and will propagate downwards. During this stage, the CO_2 replaces the pore fluid and there is a possibility for it to be irreversible, which is residual trapping. It is therefore important that the largest area possible is covered during the initial stage, as this increases the residual and solubility trapping. Finally, after multiple decades, the CO_2 will form stable minerals together with the salts that are present in the brine.

The main reaction of dissolved CO_2 involves:

$$CO_2(aq) + H_2O \leftrightharpoons H^+ + HCO_3^-. \tag{1.1}$$

Dissolved CO_2 will react with the water, forming an acidic solution. As the ionic strength of the water increases, less CO_2 is able to be dissolved. The bicarbonate can also form precipitants with cations if they are available.

In carbonate aquifers, the addition of CO_2 will dissolve the formation due to the slightly acidic solution. The dominant reaction is defined as

$$CO_2(aq) + H_2O + Calcite \leftrightharpoons Ca^{+2} + 2HCO_3^- \tag{1.2}$$

The bicarbonate can react with different cations such as Ca^{+2} and precipitate, but due to the acidic nature of the solution, bicarbonate will remain as a buffer.

In siliciclastic aquifers, the feldspar and clay present in the formation are able to react with the CO_2. The reaction pathways are diverse, but in general, the reaction is

$$Feldspar + Clay + CO_2 \leftrightharpoons Kaolinite + Calcite + Dolomite + Quartz \tag{1.3}$$

Unlike the reaction in the carbonate aquifers, there is net positive precipitation of the volume of minerals. In reactive siliciclastic aquifers, the capacity of mineralizing CO_2 is roughly double that of the carbonate or inert aquifers, only bounded by the number of cations present (Gunter, Perkins, & McCann, 1993). The disadvantage here is that these minerals could clog up the pore space, preventing further flow of dissolved CO_2. In turn, this could prevent further trapping in the reservoir.

1.1.2. Dry-out in near-wellbore region

At first, there is only the aqueous phase present in the aquifer. In the aqueous phase, multiple ions can be dissolved. When injecting dry CO_2 into an aquifer, it causes the water to evaporate into the gaseous phase. This leads to dry-out, where the total aqueous phase in the pore space is replaced by the gas phase. With the introduction of dry CO_2 in the aquifer, phase interaction is taking place, which changes the chemical composition of the pore space. A simplified diagram during the initial injection stage is shown in Figure 1.1.

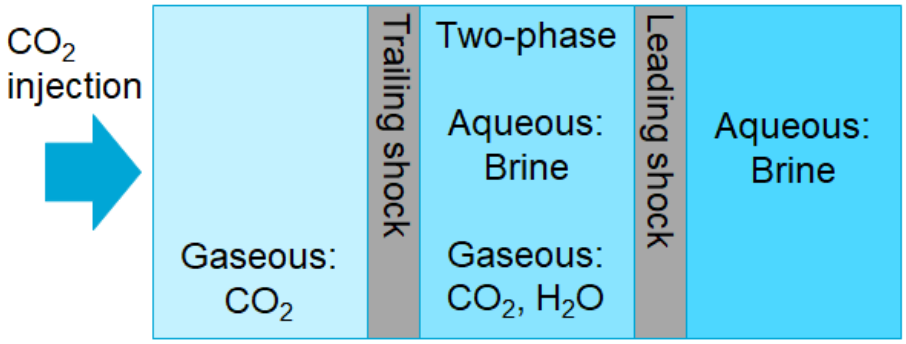

Figure 1.1: Simplified schematic of different phases present in the subsurface during initial CO_2 injection

The brine in front of the leading shock is initially pushed away. This initial brine is called the placid zone. The saturation does not vary much in this area. After the leading shock, the two-phase region is located or also named rarefaction. Here, the gaseous CO_2 interacts with the brine, evaporating the water present, but also dissolving in the brine. The dissolved CO_2 can react with the water to form carbonic acid, which decreases the pH. The evaporation of the water is due to CO_2 having a low water vapor partial pressure (Peysson, André, & Azaroual, 2014). The water will thermodynamically equilibrate and will partly vaporize to the gaseous phase. All of the water that had not been pushed away, including irreducible water in the pores, will be dried out. This could lead to the precipitation of the dissolved ions in the aqueous phase.

However, the flow of the water phase is determined by

$$U_t f_w = U_t \frac{\lambda_w}{\lambda_w + \lambda_g}(1 + \frac{\lambda_g}{U_t}(\frac{dP_c}{ds_w}\frac{\partial s_w}{\partial x}))), \tag{1.4}$$

(Roels, El Chatib, Nicolaides, & Zitha, 2016) where P_c is the capillary pressure and S_w is the water saturation. The larger the difference between the saturation, the higher the capillary backflow will be. If the capillary backflow is larger than the viscous flow, there will be a backflow, which will supply the front region with an unlimited supply of new minerals. If the brine present is slowly being dried, the water will vaporize and the minerals will precipitate on the grains. The porosity of the rock will be negatively impacted by this precipitation.

Due to pore throat restriction, not only the average porosity will decrease, but it also has a negative impact on absolute permeability, as shown by the Carman-Kozeny relationship

$$K = \Phi^2 \frac{\phi^3 D_p^2}{150(1-\phi)^2}. \tag{1.5}$$

Here K is the absolute permeability, Φ is the sphericity of the grains and D_p is the average diameter of the grains. It dictates that a decrease in porosity and an increase in the diameter of the grains will have a large negative effect on the permeability of the rock. Therefore, in the two-phase zone of our flow, if there is a significant amount of ions dissolved in the aqueous phase, there is a risk of blocking the pore space.

In turn, this will badly affect the injectivity,

$$II = \frac{Q}{\Delta P}, \tag{1.6}$$

of the aquifer as injectivity is the flow rate divided by the pressure difference. Due to pore clogging, the flow rate is decreased, so a higher pressure is needed to achieve the same injectivity index.

Increasing the pressure to create the same flow rate could lead to an increase in local pressures. Changes in stresses already pose a large fracture risk in CO_2 injection and this could lead to cap rock failure and leakage of the CO_2 (Lavrov, 2016). As the objective is to contain the gas, this would be a large failure.

1.1.3. Reservoir modeling

The disadvantage of injecting CO_2 inside of a reservoir or aquifer is the heterogeneity. Inside a reservoir, multiple phases can be present, such as natural gas and brine, but also solids. The composition of the pore space depends on the components present, temperature, and pressure. In addition to these in-situ components, with the injection of CO_2, a new phase state is formed and finally equilibrated. In order to fully understand the behavior of this system, accurate models need to be built. All of the trapping mechanisms described previously are dependent on the flow and geochemical interactions. Therefore, these models do not only need to include the flow of the CO_2 but also the interaction between chemical components.

1.1.4. Prior work

There are multiple programs for reactive transport models already made, each with its own advantages and disadvantages. The program TOUGHREACT (Xu, Sonnenthal, Spycher, & Pruess, 2006) is able to model multicomponent, multiphase reactive transport. For this, the Law of Mass Action (LMA) is applied. In our work, Reaktoro (Leal, Kulik, & Saar, 2016) is used for equilibrium chemistry which utilizes the Gibbs energy minimization (GEM) scheme. A GEM scheme (GEMS3K (Kulik et al., 2012)) has been coupled with OpenGeoSys (Kosakowski & Watanabe, 2014), especially for unsaturated flow using Richard's equation. The differences between the schemes and the coupling methods that are mostly used are described in chapter 3.

DARTS also has been coupled to create a reactive transport model, albeit in single-phase (Margert & Voskov, 2019). For this, the LMA-based PHREEQC (Parkhurst & Appelo, 2013) was used.

1.2. Scope

This study focuses on coupling DARTS with Reaktoro and modeling a multicomponent, multiphase reactive transport. For this coupling, a globally implicit algebraic framework has been made. At first, the compositional flow and transport model is made in DARTS. This provides a basis for the reactive flow and transport model.

1.2.1. Research questions

The main research question that is going to be discussed in this thesis is:

What are the implications in the near-wellbore region when dry CO_2 is being injected? Can the reactive transport be accurately modeled and quantified using the global implicit operator-based linearization approach?

This question is supported by the sub-questions:

- **How is the porosity affected by the precipitation and dissolution during CO_2 injection?**

  As described in subsection 1.1.2, during injection of dry CO_2, the ions that are in the brine can precipitate and can cause clogging of the pore space.

- **What is the effect of kinetic equilibrium on the resulting precipitation?**

  What is the effect of kinetic versus equilibrium reactions for mineral precipitation? Kinetic reactions take a rate into consideration as opposed to equilibrium.

- **Is the resulting solution physical?**

  In order to test the solution given by the coupling of DARTS and Reaktoro, it is benchmarked against an already existing reactive flow and transport solver.

2

Methodology

In this chapter, the background of the flow and transport with chemical equations and the coupling techniques used in this study are formulated. At first, the governing mass-balance equation and the thermodynamic and chemical equilibrium equations are given. Next, the Operator-Based Linearization (OBL) of DARTS is explained

2.1. Governing equation for compositional flow and transport

In order to model flow in the subsurface numerically, a reservoir is represented as a system of gridblocks. These blocks are transmissible to their adjacent neighbors, allowing fluids to flow and pressure to dissipate. The flux at the boundaries of the cell needs to be balanced, so as not to lose or gain mass without an equal mass being gained or lost. Therefore, for compositional flow, the general conservation of mass is

$$\frac{dM}{dt} = F_{in} - F_{out}, \tag{2.1}$$

where M is the mass in the cell at a certain time, F_{in} is the mass flux in the cell, and F_{out} is the mass flux out of the control volume. As M is determined as only the fluid in the pore space inside of the cell, it is a function of porosity in the reservoir. Furthermore, saturations, densities, and compositions need to be taken into the equation, since the aim is to model multiphase multicomponent flow. The resulting equation is

$$\frac{\partial}{\partial t}\left(\phi \sum_j x_{cj}\rho_j s_j\right) + div \sum_j x_{cj}\rho_j \mathbf{v}_j = \sum_j x_{cj}\rho_j (Q_j/V). \tag{2.2}$$

Here, ϕ is the porosity, x_{cj} is the molar fraction of the component in phase j, ρ_j the phase density, s_j the phase saturation, $\mathbf{v}_j$ is the phase velocity and Q_j is the phase rate. The conservation of mass for compositional flow is also true for reactive transport, as it is a mass-balance equation. This equation describes that the flow is determined by Darcy's law

$$\mathbf{v}_j = \mathbf{K}\frac{k_{rj}}{\mu_j}\left(\nabla \mathbf{p}_j - g\nabla \mathbf{z}\right), \tag{2.3}$$

where **K** is the effective permeability, k_{rj} is the relative permeability of phase j, μ is the viscosity, g is the gravity term and z is the depth.

Combining Equation 2.2 and Equation 2.3 gives

$$\frac{\partial}{\partial t}\left(\phi \sum_j x_{cj}\rho_j s_j\right) + div \sum_j x_{cj}\rho_j \mathbf{K}\frac{k_{rj}}{\mu_j}\left(\nabla \mathbf{p}_j - g\nabla \mathbf{z}\right) = \sum_j x_{cj}\rho_j (Q_j/V) \tag{2.4}$$

This equation needs to be discretized in order to be used for modeling. For this thesis, an implicit backward Euler scheme is used with finite-volume discretization. The resulting equation is:

$$\left(\phi V \sum_j x_{cj}\rho_j s_j\right)^{n+1} - \left(\phi V \sum_j x_{cj}\rho_j s_j\right)^{n} - \Delta t \sum_{l\in L}\left(\sum_j x_{cj}\rho_j T_{cj}^{l}\Delta p\right) + \Delta t \sum_j \rho_p x_{cj} Q_j = 0 \tag{2.5}$$

Where V is the volume, T_j^l the transmissibility of phase j at interface l, and p is the pressure.

2.2. Governing equation for chemical equilibrium

For thermodynamic equilibrium, an equation of state (EOS) determines whether the reactions are in equilibrium and whether there is a drive to pass to a different phase in the system. Furthermore, the second law of thermodynamics,

$$\Delta S \geq 0, \tag{2.6}$$

need to be fulfilled, where S is the entropy of the system. With each process, the entropy of the system must increase. In order to describe the optimal state for not only entropy but also enthalpy, the Gibbs energy of the system is

$$dG = -SdT + VdP + \sum_{i=1} \mu_{ci} dn_i, \tag{2.7}$$

where G is the Gibbs free energy, T the temperature, V the volume, P the pressure, μ_{ci} is the chemical potential of species i and n_i is the molar amount of species i. Comparing different states, the optimal state is where the Gibbs free energy equals $dG = 0$ or is closest to zero. This means that the equilibrium of the system is achieved.

For the chemical equilibrium, the equilibrium constant of a reaction can be used, for example for reaction aA + bB ⇌ cC + dD,

$$Q_r = \frac{[C]^c[D]^d}{[A]^a[B]^b} \tag{2.8}$$

where Q_r is the reaction quotient, the small letters are the stoichiometric coefficients and the large letters are components of the reaction. At equilibrium, the reaction quotient is equal to the equilibrium constant (K_{eq}). Using the same strategy as in the thermodynamic equilibrium, the equilibrium can be expressed in Gibbs free energy

$$\Delta G = -RT \ln K_{eq} + RT \ln Q_r, \tag{2.9}$$

where R is the ideal gas constant. If the system is at equilibrium $\Delta G = 0$. The equilibrium constants are determined by experimental measurements done at equilibrium or from standard free energy change calculations.

2.2.1. Kinetic equilibrium

In reality, every reaction takes a certain amount of time and equilibrium is not instantaneous. These reactions are kinetic and are defined as controlled by the rate of products being formed. The equation, using the same example in Equation 2.8, will be:

$$r = k[A]^a[B]^b = Ak\left(1 - \frac{\{A\}\{B\}}{K_{eq}}\right) \tag{2.10}$$

where k is the rate constant, A the area, and {A} is the activity of species A. There is a rate constant going forwards and one for reversal of the reaction. When these rate constants are the same, equilibrium is achieved. The equilibrium constant can also be calculated by multiplication of the activity of species of the equilibrated system. This means that before equilibrium, the activity of species A and B is taken and after equilibrium, the activity of the same species is taken. The ratio between these values will determine the kinetic rate.

The area is defined as:

$$A = (1 - \phi)s_s\frac{\rho_s}{\rho_T}, \tag{2.11}$$

and the rate constant can be calculated by the Arrhenius equation:

$$k = A_f e^{\frac{-E_a}{RT}}, \tag{2.12}$$

where A_f is the frequency factor and E_a is the activation energy. It describes the rate of collisions when particles collide.

For calculating the concentration of the kinetic equilibrium product, Reaktoro is not allowed to perform an equilibrium reaction. Elsewise, the concentration set by the equilibrium reaction will be altered by the kinetic rate, which will result in an over- or underestimation of the actual kinetic concentration. Therefore, the kinetic reaction product is decoupled and identified not as a component, but as species. Reaktoro will therefore determine the flash and the other equilibrium reactions.

During transport, if the time steps are small, equilibrium cannot be assumed and a kinetic rate has to be given for the reaction to accurately give the resulting chemical equilibrium. If the rate is such that the time to reach equilibrium is achieved, it can be assumed that the reaction is instant. It is more accurate to use equilibrium constants than kinetic rates, which are mostly empirical and measured under certain circumstances.

2.3. Compositional flow

Initially, a compositional model is built using both an implicit and explicit approach. This model will provide a stepping stone to reactive transport, as the equations for flow and interaction between phases are of the same approach. In this compositional model, the framework used by DARTS, namely Operator-Based Linearization (OBL) will be applied.

2.3.1. Compositional model

In order to better understand the transport physics behind a reactive transport solver, a simple compositional flow simulator using the OBL approach is made. For this, the conservation

equation in Equation 2.2 is simplified

$$z_c = \frac{\rho_c}{\rho_T} = \frac{\sum_j x_{cj}\rho_j s_j}{\sum_j \rho_j s_j}, \tag{2.13}$$

with z_c the molar fraction of component c, ρ the density of component or the total, x_{cj} the molar fraction of component c and phase j, and s_j is the phase fraction of phase j. This allows rewriting the mass-conservation equation in terms of molar fraction.

Writing the residual form of the discretized Equation 2.5 in 1D gives:

$$r_{c,i} = \frac{V}{\Delta t}(\phi\rho_T z_c)_i^{n+1} - (\phi\rho_T z_c)_i^n + T_c^w(p_i - p^w) - T_{c,i+\frac{1}{2}}(p_{i+1} - p_i) + T_{c,i-\frac{1}{2}}(p_i - p_{i-1}) = 0, \tag{2.14}$$

where V is the volume of the cell, Δt the time step, ϕ the porosity, ρ_T the total density, T_c^w the transmissibility between the cells and the well, T_c the transmissibility between cells and p the pressure. In this simplified model, we assume that there is no loss between the well and the cell, therefore this value is set to zero. This equation can be simplified using

$$T_{c,i+\frac{1}{2}}(p_{i+1} - p_i) = -U_t\rho\frac{x_c\lambda_o + y_c\lambda_g}{\lambda_o + \lambda_g}_{i+\frac{1}{2}} = -U_t\rho F_{c,i+\frac{1}{2}}, \tag{2.15}$$

where U_t is the total velocity and λ is the phase mobility. The fraction can be simplified using F_c, which is Buckley-Leverett fractional flow. Using this simplification and rewriting gives

$$-U_t\rho(F_{c,i+\frac{1}{2}} - F_{c,i-\frac{1}{2}}) = \frac{\Delta x}{\Delta t}\phi(z_{c,i}^n - z_{c,i}^n). \tag{2.16}$$

To simplify this even further, a dimensionless Θ can be introduced, which equates to:

$$\Theta = \frac{U_t\Delta t}{\phi\Delta x}, \tag{2.17}$$

and all together, the residual is simplified to:

$$r_{c,i} = (\rho_T z_{c,i}^{n+1} - \rho_T z_{c,i}^n) + \Theta\rho(F_{c,i+\frac{1}{2}} - F_{c,i-\frac{1}{2}}). \tag{2.18}$$

Now, the residual is a function of molar fraction, fractional flow, and Θ. These dependencies can also be translated to nonlinear operators. For example, it can be rewritten as

$$r_{c,i} = (\alpha_i^{n+1} - \alpha_i^n) + \Theta(\beta(z_i^{n+1}) - \beta(z_{i-1}^{n+1})), \tag{2.19}$$

which is the residual in operator form. The operators can be used to introduce physics into the system. In this example, the operators are

$$\alpha_{c,i} = \rho_T z_{c,i}, \quad \beta_{c,i} = \frac{\frac{\rho_w x_c S^{n_{s1}}}{\mu_w} + \frac{\rho_g y_c(1-S^{n_{s2}})}{\mu_w}}{\frac{S^{n_{s1}}}{\mu_w} + \frac{(1-S^{n_{s2}})}{\mu_g}}, \tag{2.20}$$

where S is the saturation, n_s the saturation exponent, and μ the viscosity of the phase. Here, β_c is written for a two-phase system, with k_r being the relative permeability and mu the viscosity. Furthermore, β_c is taken by the upstream cell, so there is β_{minus} and β_{plus} depending on where the flow comes from. Using these operators simplifies the problem, as these describe the fluid and rock properties. These operators allow for all physics to be contained in a functional form.

2.3.2. Rachford-Rice equation

The molar fraction of both phases can be calculated using flash. For this, a constant K-value Rachford-Rice flash is used. The flash calculation is done with the following equation:

$$\sum_{c=1}^{n_c} \frac{z_c(K_c - 1)}{1 + \nu_g(K_c - 1)} = 0, \tag{2.21}$$

where ν_g is the phase fraction, which is the relationship between gas and total flow. ν_g is found using the bisection method, as there is a guarantee for convergence with this method. If the value of ν lies between 0 and 1, the component is in two-phase. A value above one is the gaseous phase and below is solely the aqueous phase. The molar fraction of a phase is calculated with:

$$x_c = \frac{z_c}{\nu_g(K_c - 1) + 1}, \quad y_c = x_c K_c, \tag{2.22}$$

where x_c is the liquid fraction and y_c is the gas fraction of component c. The summation of the phase fractions always equals one for each component.

2.3.3. Newton-Raphson method

Since Equation 2.19 is a nonlinear system, there is a need to linearize it in order to solve the problem. As the residual is defined for the problem, it is solved using the Newton-Raphson method. The main equation is as follows:

$$r^{\nu} + \mathbf{J}^{\nu} * \delta z^{\nu+1}, \tag{2.23}$$

where r is the residual, **J** is the Jacobian matrix, all at nonlinear iteration ν. To solve the system, we have an initial guess of z^{ν}, so $R(z^{\nu})$ can be updated. Next $\delta z^{\nu+1}$ is found by setting

$$\delta z^{\nu+1} = (\mathbf{J}^{\nu})^{-1} * (-R^{\nu}), \tag{2.24}$$

and with this new $\delta z^{\nu+1}$, $z^{\nu+1} = z^{\nu} + \delta z^{\nu+1}$. This is iterated until the difference is smaller than the set tolerance and the solution is met.

2.3.4. Jacobian

For the Newton-Raphson method, a block-sparse Jacobian needs to be made for the nonlinear system. It is filled using:

$$\frac{\partial r_i}{\partial z_{i-1}} = -\Theta \frac{\partial \beta}{\partial z}(z_{i-1}), \quad \frac{\partial r_i}{\partial z_i} = \frac{\partial \alpha}{\partial z}(z_i) + \Theta \frac{\partial \beta}{\partial z}(z_i). \tag{2.25}$$

For each of z_c components, a block needs to be created for each cell in the discretized reservoir. An example of a three-component system with three cells is

$$\begin{bmatrix} \frac{\partial \alpha_1}{\partial z_1} + \Theta \frac{\partial \beta_1}{\partial z_1} & \frac{\partial \alpha_2}{\partial z_1} + \Theta \frac{\partial \beta_2}{\partial z_2} & 0 & 0 & 0 & 0 \\ \frac{\partial \alpha_3}{\partial z_1} + \Theta \frac{\partial \beta_3}{\partial z_1} & \frac{\partial \alpha_4}{\partial z_2} + \Theta \frac{\partial \beta_4}{\partial z_2} & 0 & 0 & 0 & 0 \\ -\Theta \frac{\partial \beta_1}{\partial z_1} & -\Theta \frac{\partial \beta_2}{\partial z_2} & \frac{\partial \alpha_1}{\partial z_1} + \Theta \frac{\partial \beta_1}{\partial z_2} & \frac{\partial \alpha_2}{\partial z_1} + \Theta \frac{\partial \beta_2}{\partial z_2} & 0 & 0 \\ -\Theta \frac{\partial \beta_3}{\partial z_1} & -\Theta \frac{\partial \beta_4}{\partial z_2} & \frac{\partial \alpha_3}{\partial z_1} + \Theta \frac{\partial \beta_3}{\partial z_2} & \frac{\partial \alpha_4}{\partial z_1} + \Theta \frac{\partial \beta_4}{\partial z_2} & 0 & 0 \\ 0 & 0 & -\Theta \frac{\partial \beta_1}{\partial z_1} & -\Theta \frac{\partial \beta_2}{\partial z_2} & \frac{\partial \alpha_1}{\partial z_1} + \Theta \frac{\partial \beta_1}{\partial z_2} & \frac{\partial \alpha_2}{\partial z_1} + \Theta \frac{\partial \beta_2}{\partial z_2} \\ 0 & 0 & -\Theta \frac{\partial \beta_3}{\partial z_1} & -\Theta \frac{\partial \beta_4}{\partial z_2} & \frac{\partial \alpha_3}{\partial z_1} + \Theta \frac{\partial \beta_3}{\partial z_2} & \frac{\partial \alpha_4}{\partial z_1} + \Theta \frac{\partial \beta_4}{\partial z_2} \end{bmatrix}, \quad (2.26)$$

With more components, this matrix would also increase in size, by $n - 1$. Solving this matrix is computationally expensive, especially when the number of components is increased.

2.3.5. Implicit and explicit compositional model

The compositional model can be implemented in an implicit or explicit manner. The implicit method, as shown in Equation 2.5. The advantage of using the implicit method is:

- Unconditionally stable method
- Timestep is not restricted
- Very efficient linear and nonlinear solvers

However, there are also some disadvantages:

- Nonlinear solution with full Jacobian construction
- Not unconditionally convergent
- Expensive if time is not chosen effectively

Solving a compositional system with three components is shown in Figure 2.1. In this figure, the same system is solved using an implicit backward Euler method and an explicit forward Euler method.

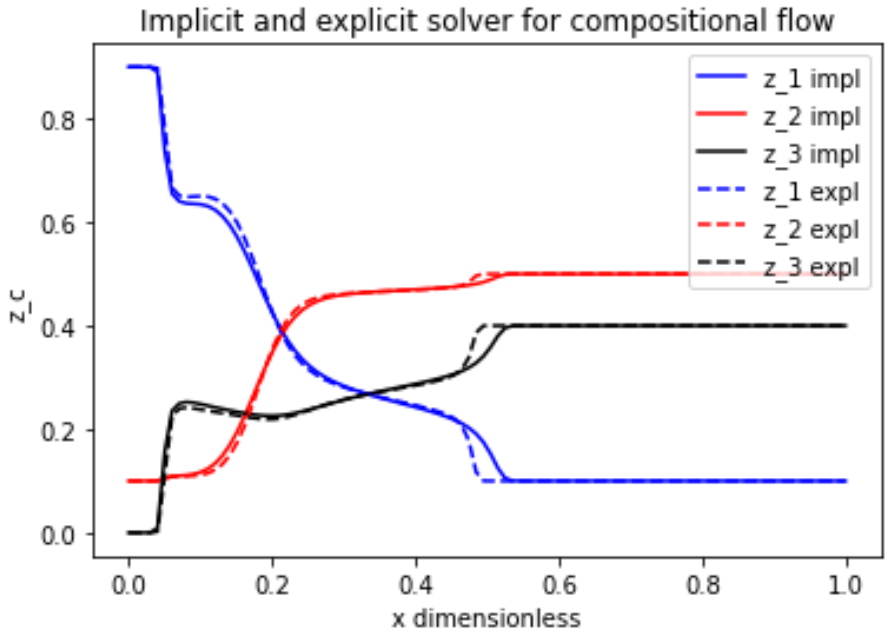

Figure 2.1: Implicit and explicit compositional flow

The main difference is that the implicit method has smearing of the shocks, due to using the values from neighboring cells when calculating the solution. This results in the shocks being smoother for the implicit method. Increasing the resolution of the reservoir would improve the sharpness of the shocks, as the difference between cells is smaller. For the explicit method, there is only a single diagonal in the block-sparse Jacobian, which is computationally efficient.

2.4. Component- to element-based transport

Before switching to a reactive transport model, the components of the model need to be replaced by their respective elements. Here, we define elements as the smallest subset of components, defined by the user. For example, the mineral calcite can be divided into Ca^{+2} and CO_3^{-2} ions. Another option would be to use chemical elements and calcite would be defined as Ca, C, and O elements. Therefore, species can be used as elements in this methodology.

Transporting chemical components of reactants generates a stiff equation and therefore, for better numerical control, components are separated into elements for transport. This means that DARTS solely works in the element space to achieve numerically stable solutions and Reaktoro will convert the elements into components. For this, Reaktoro will equilibrate the element system in the component space, resulting in components. In a reactive transport problem, there are two types of chemical reactions, namely equilibrium and kinetic. In theory, equilibrium reactions can also be described as kinetic. However, as kinetic reaction speeds are mostly empirical, it is better to define two types of reactions. The assumption is made that these reactions are linearly independent. These can be defined as:

$$0 \rightleftarrows \sum_{i=1}^{N} v_{ir} n_i, \tag{2.27}$$

where v_{ir} is the stoichiometric matrix of the i-th species of the r-th reaction and n_i the molar amount of the i-th species (Lichtner, 1985). The stoichiometric matrix describes the system in terms of both equilibrium and kinetic reactions for both homogeneous and heterogeneous chemical reactions. This matrix can also be written as:

$$\overline{\mathbf{S}}_{n_c \times n_r} = \begin{bmatrix} \mathbf{S}_{eq} & \mathbf{S}_k \end{bmatrix} = \left[\begin{array}{c:c} \mathbf{0}_{n_e q \times n_k} & -\mathbf{I}_{1,n_e q \times n_q} \\ -\mathbf{I}_{2,n_k \times n_k} & \mathbf{S}_{1,n_k \times n_e q} \\ \hline \mathbf{S}_{2,(n_c - n_r) \times n_k} & \mathbf{S}_{3,(n_c - n_r) \times n_e q} \end{array}\right], \tag{2.28}$$

where the canonical stoichiometric matrix $\overline{\mathbf{S}}$ of size n_c, which is the amount of components, by n_r, the number of reactions (Molins, Carrera, Ayora, & Saaltink, 2004). It is composed multiple matrices $\mathbf{S}_1$, $\mathbf{S}_2$, $\mathbf{S}_3$ and identity matrices $\mathbf{I}_1$, $\mathbf{I}_2$. These are sized by n_{eq}, the number of equilibrium reactions, and n_k, the number of kinetic reactions. On the left of the vertical dashed line, the kinetic reactions are placed, whereas, on the other side, all of the equilibrium reactions are stored. On top are the reactants and underneath are the products of the reactions. Therefore, this matrix shows all of the reactions possible in the system, with their reactants and products.

Next, the elimination matrix is introduced, which is composed of all the elements in the system and can therefore be described as:

$$\mathbf{ES} = \mathbf{0}, \tag{2.29}$$

and through this relation, the elimination matrix is defined as

$$\mathbf{E} = \begin{bmatrix} \mathbf{E}_1 \\ \mathbf{E}_2 \end{bmatrix} = \begin{bmatrix} \epsilon_{1,1} & \epsilon_{1,2} & \cdots & \epsilon_{1,n_c} \\ \epsilon_{2,1} & \epsilon_{2,2} & \cdots & \epsilon_{2,n_c} \\ \vdots & \vdots & \vdots & \vdots \\ \epsilon_{n_e,1} & \epsilon_{n_e,2} & \cdots & \epsilon_{n_e,n_c} \end{bmatrix}, \tag{2.30}$$

and it denotes which component is composed of which elements.

During transport, the components have to be switched to elements. Using the elimination matrix, the equation becomes:

$$z_e \sum_c \sum_e e_{ec} z_c - \mathbf{Ez} = 0 \tag{2.31}$$

Where z_e is the mole fraction of the element, e is the element of the component in the elimination matrix, z_c is the mole fraction of the component, E is the elimination matrix and z is the mole fraction. When this element-based molar fraction is used as input for Reaktoro, it will equilibrate into components.

For density, the equation is similar:

$$\rho_T^e = \sum_{j=1}^{P} \left(\rho_j s_j \sum_{c=1}^{C} \sum_{e=1}^{E} e_{ec} x_{cj} \right), \tag{2.32}$$

where the total element-based density is a function of the saturation and density of each phase and a sum of the elimination matrix multiplied by the component molar fraction of each phase. For each phase, the density of the components is converted to density by elements.

2.5. Operator-Based Linearization approach

In order to solve the Jacobian in Equation 2.26, all the partial derivates need to be analytically derived, which is computationally expensive. With OBL, these derivates are derived from interpolations, which are easier to solve. At first, the operators from Equation 2.20 will be used as a basis. As transport only happens in the element space, the operators need to be defined in the element space. Therefore, the operators become after using Equation 2.31 and Equation 2.32:

$$\alpha_i = (1 + c_r(p - p^0))\rho_e z_e, \tag{2.33}$$

$$\beta_i = \sum_c (e_{ic} \times \sum_p x_c j \rho_j \frac{k_{rj}}{\mu_j}). \tag{2.34}$$

Using Newton-Raphson method

$$\mathbf{J}(z^{n+1,k})(z^{n+1,k+1} - z^{n+1,k}) = -r(z^{n+1,k}), \tag{2.35}$$

with k being the Newton iteration and

$$\mathbf{J} = \frac{\partial r_i}{\partial z_j}. \tag{2.36}$$

In the OBL approach, the α and β operators are estimated using interpolation. For the pressure and molar fractions, a grid is introduced, named P and $\mathbf{Z}$, where P is composed of the range of pressures in the system, and $\mathbf{Z}$ is the molar compositions changing between 0 and 1. The parameter space becomes of the problem $\{p, z_1, ..., z_{nc-1}\}$. Within this set, each vertex is calculated of the parameter space and when the p and $\boldsymbol{z}$ fall in a grid cell, the solution is interpolated. The interpolation becomes:

$$\hat{\alpha_e}(p, z) = F_{\alpha_e}(p, z), \quad \hat{\beta_e}(p, z) = F_{\beta_e}(p, z). \tag{2.37}$$

Using $\alpha_{i,j} = \alpha_{P_i, Z_j}$, the piecewise linear interpolation is defined as:

$$F_{\alpha_e}(p, z) = (1 - z_j)((1 - p_i)\alpha_{i,j} + p_i\alpha_{i+1,j}) + z_j((1 - p_i)\alpha_{i,j+1} + p_i\alpha_{i+1,j+1}). \tag{2.38}$$

The partial derivative for the Jacobian can be found as a coefficient of the interpolation:

$$\frac{\partial F_\alpha}{\partial p} = \frac{(1 - z_j)(\alpha_{i+1,j} - \alpha_{i,j}) + z_j(f_{i+1,j+1} - \alpha_{i,j+1})}{P_{i+1} - P_i}, \tag{2.39}$$

$$\frac{\partial F_\alpha}{\partial z} = \frac{(1 - p_i)(\alpha_{i,j+1} - \alpha_{i,j}) + p_i(\alpha_{i+1,j+1} - \alpha_{i+1,j})}{Z_{j+1} - Z_j}. \tag{2.40}$$

The same can be applied to the β operator and other operators (Voskov, 2017). This means that all nonlinear physics can be interpolated using this method, which results in a Jacobian composed of linear operators.

Using this method greatly simplifies the calculation of the Jacobian, even as it can be more inaccurate than the analytical method. The number of points in the parameter space determines the accuracy of the method.

2.5.1. Adaptive parametrization

As most points will never be used in the simulation, in order to save time, not all points need to be generated inside the parameter space. Especially in multicomponent systems, such as described in this thesis, most of the parameter space will not be used, as some concentrations will never go above a certain threshold. The individual grid cells in parameter space will only be prepared when necessary and their vertices saved for later use. As the grid cell share vertices, the vertices are stored and called when a grid cell is made. With this method, the same vertex does not need to be recalculated for all grid cells sharing it. If the parameter space is built up efficiently, overall performance is improved significantly (Khait & Voskov, 2018).

3

Geochemical solvers

In this Chapter, a short description of the geochemical solvers PHREEQC and Reaktoro is given. At first, the law of mass action (LMA) method of PHREEQC is explained and in the next section the Gibbs energy minimization (GEM) of Reaktoro. Most reactive transport models are using the LMA approach, which is easy to implement but less flexible than the GEM approach.

3.1. PHREEQC

PHREEQC (Parkhurst & Appelo, 2013) is a geochemical solver that can perform transport modeling with multiphase, multicomponent, reversible, and irreversible reactions, with a mix of equilibrium and kinetic controlled reactions. To perform the equilibrium calculation, it uses the Law of Mass Action (LMA) method, which is described as:

$$\ln K_r = \sum_{i=1}^{N} v_{ir} \ln \alpha_i (r = 1, ..., R), \tag{3.1}$$

where K_r is the equilibrium constant of the rth reaction, v_{ir} is the stoichiometric matrix of the i-th species of the r-th reaction, which can be both positive and negative depending on the species being a product or a reactant, α_i is the activity and N is the number of species.

The disadvantage of this method is that with non-ideal multicomponent phases, the results are not accurate due to data in the databases. Furthermore, in this method, equilibrium is set as a constraint, so the nonlinear iteration is allowed to adjust the mass of the species until mass balance is acquired (Steefel & MacQuarrie, 1996). These adjustments of mass can lead to non-convergence.

3.2. Reaktoro

Reaktoro (Leal, Kulik, & Saar, 2016), is also a geochemical solver, but it differs in how it calculates the chemical equilibrium. Unlike PHREEQC, Reaktoro uses the Gibbs energy minimization (GEM) method. With this method, the total Gibbs free energy of the system is minimized

with the constraints of temperature, pressure, and molar amount of the species (Leal, Kulik, & Kosakowski, 2016). The minimization of Gibbs energy is described as:

$$G = \sum_{i=1}^{N} n_i(\mu_i^\circ + RT \ln \alpha_i), \tag{3.2}$$

where G is the Gibbs energy of the system, n_i is the molar amount of the ith species, μ_i° is the standard chemical potential of the ith species and α_i is the activity of the ith species. The activity of the species is dependent on the phases the species is present in and what phases are present. Using a minimization scheme, the chemical equilibrium of the system can be found. The advantage of this method is that it is capable of estimating the stable phases even for extreme non-ideal behavior (Karpov, Chudnenko, & Kulik, 1997).

3.3. Coupling methods

The reactions and transport are intertwined with each other. As the concentrations of species change, so do the fluxes of these species. The other way around is also true, a change in flux means a change in reaction rates. The easiest way to model reactive transport is to assume a constant, single velocity, and the reactions are described in a first-order rate law (Steefel & MacQuarrie, 1996) so that the solution becomes linear. To model without these assumptions, the problem becomes non-linear, which can be solved using the Newton-Raphson method or another scheme.

In most systems, there is a mix between equilibrium and kinetic reactions, which provides problems to the differential-algebraic system of equations (Steefel & MacQuarrie, 1996). Therefore, the transport and chemical reactions are decoupled most of the time, named operator splitting. With this method, the equilibrium and kinetic reactions

3.3.1. Sequential non-iterative approach

The sequential non-iterative approach (SNIA) is an operator-splitting approach. A single time step is composed of transport at first and a chemical equilibrium reaction second (Steefel & MacQuarrie, 1996). Therefore, this implies that the solution is added to the next cell instantaneously and the reaction happens afterward.

For equilibrium reactions, this does not pose much trouble, but for kinetic reactions it does. There is a mass balance error for continuous mass influx boundary conditions. Once the transport is completed and the chemical reactions are considered, the composition that is present in the cell for the entire time step, before transport, had more time inside the cell than the recently added composition. As kinetic reactions are a function of time, it should be considered that the transported composition had a different amount of time inside the cell than the original composition (Valocchi & Malmstead, 1992). One solution to this problem is to take small time steps, but will greatly increase the time it takes to give the final result. The order of splitting can also be reversed at each time step to compensate for the error.

3.3.2. Sequential iterative approach

In the sequential iterative approach (SIA), the transport equations and the chemical equilibrium equations are separate from each other, which is similar to the SNIA. As the previous approach had an error due to the operator splitting at continuous boundary mass fluxes, this method couples the transport and chemical reaction by iterating between the two terms (Yeh & Tripathi, 1991). Iteratively, the reactive transport equation is evaluated with switching terms as a source term. If the error of the concentration is below the tolerance, the solution is met and the following time step is allowed. In this case, the error from the operator splitting, which can happen in the SNIA, is avoided. However, going to the next time step depends on the tolerance and if that is set too strict, no solution can be found and the transport equation does not converge. Therefore, this method can achieve higher numerical accuracy, with the downside of being more computationally expensive the more iterations are being performed.

3.3.3. Global implicit approach

In the global implicit approach (GIA), the reaction and transport are solved during a single time step, so the solution is not split anymore. It is very flexible and is able to take large time steps. The advantage is that no separate system needs to be created for the chemical reaction terms, however, this also means that it is computationally more expensive, as the nonlinear system becomes much larger (Knodel, Kräutle, & Knabner, 2022).

Comparing GIA to the sequential approaches put GIA at high numerical accuracy against higher computational expenses(Beck, Rinaldi, Flemisch, & Class, 2020).

3.4. Simplified reactive model

In order to show that coupling between Reaktoro and the OBL approach is possible, a simple model is made, where only the accumulation and flux terms are used for transport physics. For this implementation, the GIA is chosen, as described in subsection 3.3.3, as it will increase the numerical accuracy. The computational speed is of less importance, as OBL will increase the performance. The major computations of Reaktoro need to be done only once, as the vertices are saved for further use, as described in subsection 2.5.1. The simplification made in this model are:

- Constant velocity
- Instaneous equilibrium
- No capillary
- Flow is linear and horizontal
- Incompressible
- Immiscible phases
- Isothermal
- Ideal chemical solutions

With these simplifications in physics, the focus is on the coupling between OBL and Reaktoro. At first, a simple reaction is modeled, in a single phase. The distribution of species according to equilibrium is done by Reaktoro, as the phase distribution.

3.4.1. Coupling Reaktoro with transport solver

To model flow in the simplified OBL model, the variables of phase fractions, molar phase fractions, molar fractions, and density need to be known. These values need to be computed by Reaktoro for each cell. This information is passed to the transport code, which will calculate a single timestep and return to Reaktoro for a new computation of these variables. As the transport is using molar fractions and Reaktoro cannot handle these values as input, it is assumed that the moles of a species is equal to the molar fraction. With this method, the relative differences remain and for the transport, the moles are translated back to molar fractions.

Reaktoro will therefore be used as a replacement for the Rachford-Rice flash, where it is able to compute what components are in a certain phase and which reactions happen.

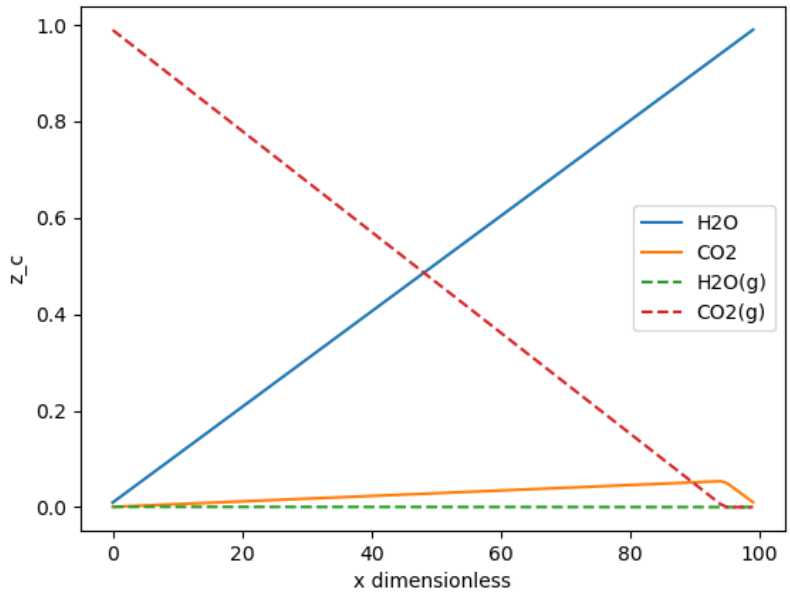

Figure 3.1: Two-phase interaction of H_2O and CO_2 at different concentrations at 200 bar and 320 Kelvin

In Figure 3.1, different concentrations of H_2O and CO_2 are added in different cells, without transport, in stand-alone Reaktoro. Here, both components are added to the aqueous phase and allowed to enter the gas phase. As shown, the concentration of CO_2 in the aqueous phase increases, until the H_2O is saturated with CO_2. The concentration of H_2O in the gas phase is almost negligible, at roughly 0.005 moles to a total of 1 mole in a cell.

In Reaktoro, each mineral is assigned its own phase, but during transport, the solid phase is a single phase. Therefore, in transport, the solid phase can be composed of multiple solid minerals. The relative saturation is calculated using the volume calculated by Reaktoro. As Reaktoro has no knowledge of the transport and of which cell it is in, it estimates the volume

using partial molar fractions at certain pressure and temperature of each component.

The density is calculated using the partial molar volume calculated by Reaktoro and the mass of the elements added to the system. These values are taken from a database. As described earlier, the exact moles are not known, only the molar fractions. Even with this relative quantity of moles, the density is calculated accurately.

For the phase fractions, the relative saturation of each phase needs to be known. Using the partial molar volumes from the density calculation, the relative saturation is calculated as:

$$s_j = \frac{V_j}{V_{tot}}, \tag{3.3}$$

and with this relative saturation for each phase, the phase fraction in terms of density is

$$\nu_j = \frac{n_j}{n_{tot}} = \frac{\rho_j s_j}{\sum_{j=1}^{J} \rho_j s_j}, \tag{3.4}$$

and then these phase fractions need to be checked. If the phase fraction of the aqueous or gaseous phase is near or equal to zero, it is taken out, so the number of phases is decreased. The solid phase however needs to be always present, even as it might be in a small quantity. This is due to the fact that DARTS works with trace amounts.

The molar phase fractions are calculated by dividing the moles of a component by the total mole in a certain phase. If the component does not exist in a certain phase, the value of the molar phase fraction for that component will be zero. For each phase, the molar phase fraction will equal one and therefore it shows easily the relative quantities of each component in each phase.

The molar fractions are calculated in a similar fashion as the molar phase fraction, however, here the quantity of a component in all phases is divided by the total mole in the system.

The input values for Reaktoro are the elements coming from transport. It can be defined which component can exist in what phase and also which component is allowed to form. Using equilibrium reactions, Reaktoro will output the result in components. As Reaktoro works with a different cut-off value than the transport part, the newly acquired molar fractions need to be at least the minimum value set by the transport code. Once the transport is finished, the minimum value can be extended again also to incorporate Reaktoro's minimal value to keep everything consistent. Otherwise, Reaktoro will equilibrate a system with a component at a higher concentration.

3.4.2. Single-phase reactive transport

The code is coupled with Reaktoro for a simple one-phase transport model. At first, Reaktoro needs to be initialized by a database, for example, the PHREEQC standard database. With this database, Reaktoro has all the information it needs to create a chemical equilibrium with the elements given. Each cell will have its own separate chemical system, which can be altered. Transport of elements is completely decoupled from Reaktoro, it only has information of the set $\{p, z_0, z_1, ..., z_{nc-1}\}$ at a specific time. After Reaktoro has equilibrated the system, the components need to be translated back into elements before transport.

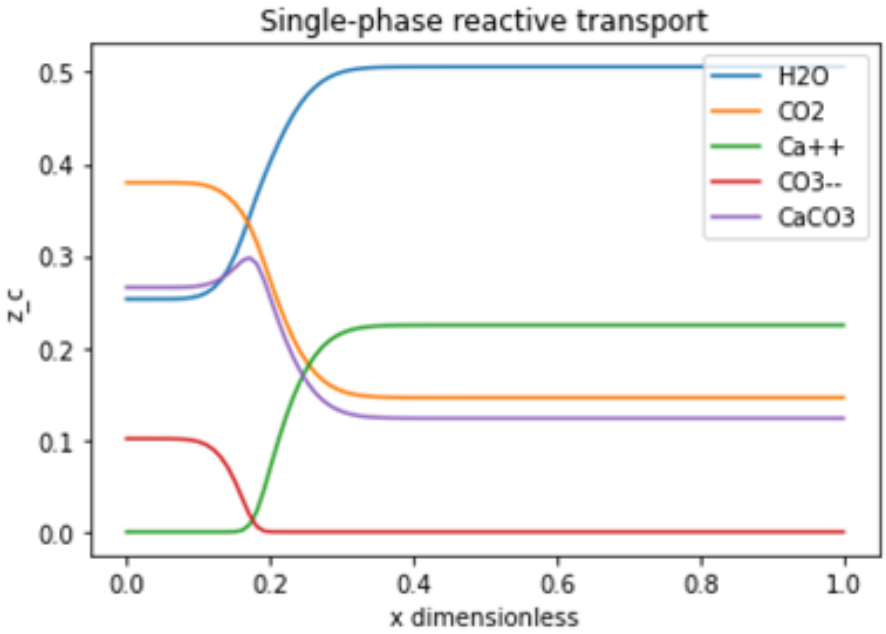

Figure 3.2: Single phase transport with reaction Ca^{+2} + CO_3^{-2} ⇌ $CaCO_3$(aq)

In Figure 3.2, the simplified model is shown. There is only a single reaction, namely: Ca^{+2} + CO_3^{-2} ⇌ $CaCO_3$(aq) and there is only a single phase. Furthermore, the effect of pH is not modeled, even as it might change during the injection. At the shock front, the concentration of $CaCO_3$(aq) is increased, as this is the cross-over of the concentration of calcium and carbonate ions. Precipitation is not allowed here, so the solids are able to move along with the water.

In Reaktoro, it is allowed to have an influence on the reactions that are possible within the system. In Figure 3.2, H^+ is not a component that is specified and is therefore not allowed to form. Furthermore, even when H^2 is specified, if HCO_3^- is not specified, H^+ will not react and CO_3^{-2} will not act as a buffer. It is possible to specify that all components containing a certain element will be utilized, which will result in multiple components with reactions. In order to have total control for simple solutions, the specification of species and components is necessary.

3.5. Reactive model in DARTS

Starting with a compositional model inside DARTS, the aim is to model reactive flow with the help of Reaktoro. Reaktoro will handle the flash and reactions inside the cells, whereas DARTS will handle the flow between control volumes. The first building block that is needed, is Reaktoro itself. In order to couple Reaktoro, DARTS needs to be changed to an element-based instead of component-based transport due to the stiffness of component-based transport.

3.5.1. Operators in DARTS

For the flow and transport of elements, the Jacobian is filled with multiple operators. First, is the accumulation term (α), which describes the rate of mass that remains inside the cell. It is

calculated as

$$\alpha = c_r \rho_T^e z_e \phi, \tag{3.5}$$

where c_r is the rock compression. For the accumulation term, the values of ρ_T^e and z_e are used before the equilibration by the geochemical solver. This is to maintain mass balance. Here ρ_T^e is calculated according to Equation 2.32. The porosity is defined as:

$$\phi = \phi_{tot}(1 - \frac{s_s \rho_s}{\rho_t}), \tag{3.6}$$

since in the accumulation term, the solids are also considered. The treatment of porosity is defined as the volume of the solids that are occupying the pore space. If there are no solids present, the porosity remains constant. As described in Equation 1.5, a change in porosity will also mean a change in permeability. In the accumulation term, porosity change due to the compressibility of the rock is also taken into account by the compressibility factor.

Next, the flux term (β), describes the mass that flows through the control volumes. The equation only takes into account the non-solid phase, as the solid phase is unable to be transported and should have no flux. The equation becomes:

$$\beta_c = \frac{x_{cj} \rho_j k_{r_j}}{\mu_j}, \tag{3.7}$$

which takes into account the components. In order to use the flux operator, the operator itself will be changed to element-space by

$$\beta_e = \sum_c \sum_e e_{ec} \beta_c, \tag{3.8}$$

which changes the operator from component to element space. Using this method, the other operators can remain standardized and no additional complications need to be added to the individual operators. Each operator that is in the component space, can be modified easily to work in the element space.

Finally, the γ, χ, and δ operators are calculated. The first two operators are for diffusion, one for diffusion inside the gradient, and one for diffusion outside of the gradient. The δ operator is used for the kinetic rate for certain reactions in case it is necessary.

Reaktoro allows for the calculation of the kinetic rate. For this, the activity of each species needs to be known, which is taken from a database. The activity can be calculated according to Equation 2.10. Using the kinetic rate value, the solution can be calculated within the flow and transport evaluation. However, the kinetic product cannot perform as a component of a species and needs to be included as a species. This is due to DARTS calculating the concentration of the kinetic product.

4

Results

For the results chapter, the parameters chosen for the reservoir and pressure-volume temperature (PVT) are given in Table 4.1. The database used in these examples is from the PHREEQC.dat file and the ideal thermodynamic activity model is used. At first, simple single-phase models are shown, after which the results of the multiphase precipitation are presented. Porosity treatment in the single- and multiphase will be discussed. Furthermore, a kinetic reaction problem and a 2D problem are shown. A pH problem is also given and at the end, a multiphase and a pH problem will be benchmarked with MoReS coupled with PHREEQC.

Parameters reservoir	**Value**	**PVT**	**Value**
Cell size	10x1x1 m	Initial pressure	100 bar
Porosity	0.2	Injection / production pressure	105 / 95 bar
Permeability x, y, z	100, 100, 10 mD	Temperature	320 Kelvin
Depth	2000 m	Viscosity fluid / gas	1 / 0.1 cP
Rock compressibility	1e^{-5} bar^{-1}	K_{re} / n	1 / 2

Table 4.1: Reservoir and PVT data used in general results

The relative permeabilities and the Brooks-Corey exponent n are kept equal for all phases.

4.1. Single-phase dissolution case

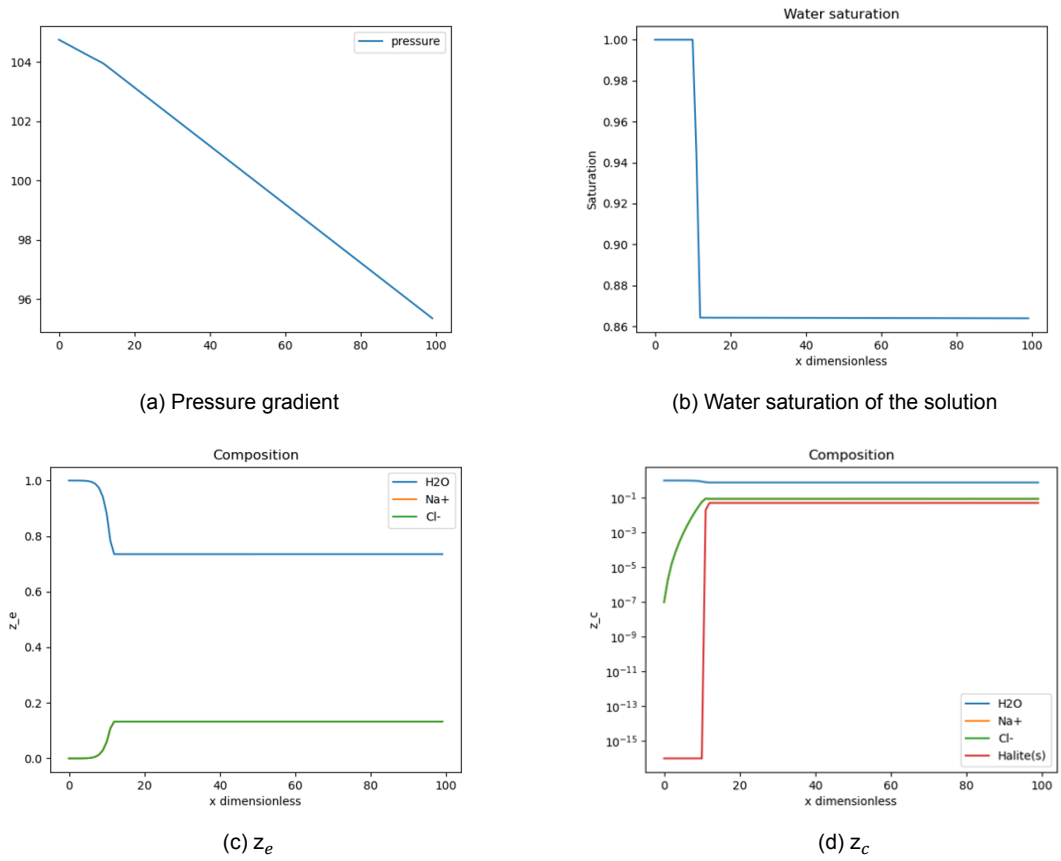

(a) Pressure gradient

(b) Water saturation of the solution

(c) z_e

(d) z_c

Figure 4.1: 1D dissolution of precipitated salt, injection of pure H_2O in brine

For Figure 4.1, the initial reservoir condition is a saturated brine, where a small amount of halite is precipitated. Initially, the concentration of Na^+ and Cl^- ions are ten molal each. The reservoir and PVT parameters follow Table 4.1. The pure water injected into the reservoir will dissolve the precipitated mineral and dilute the ion concentrations. The shock is located at cell 12, which happened after running the simulation for 300 days.

4.2. Multiphase precipitation case

In this model, CO_2 gas is injected into a brine, and the following reactions can occur:

$$\begin{aligned} H_2O(aq) &\rightleftharpoons H_2O(g), \\ CO_2(aq) &\rightleftharpoons CO_2(g), \\ Ca^{2+}(aq) + CO_3^{2-}(aq) &\rightleftharpoons CaCO_3(s), \end{aligned} \tag{4.1}$$

where calcite is in the solid phase, which is allowed to precipitate when the water is super-saturated. Initially, there is 0.8 M Ca^{+2} and 0.8 M CO_3^{-2} present. Dry CO_2 is injected into the reservoir for 500 days, which is shown in Figure 4.2. The reactions are all equilibrium reactions in this example.

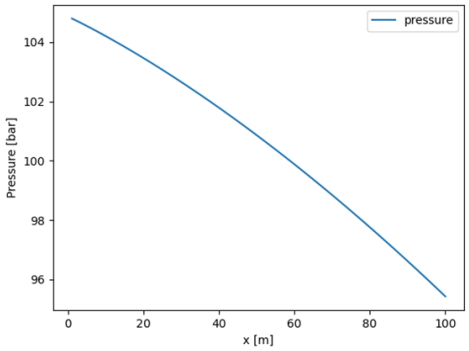

(a) Pressure gradient

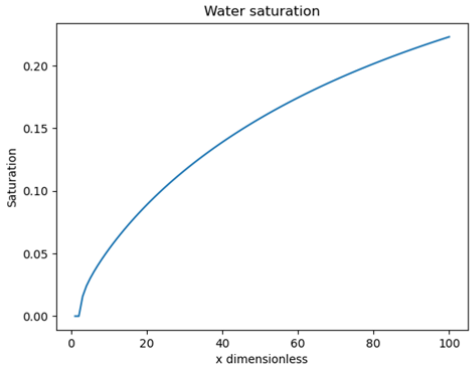

(b) Water saturation of the solution

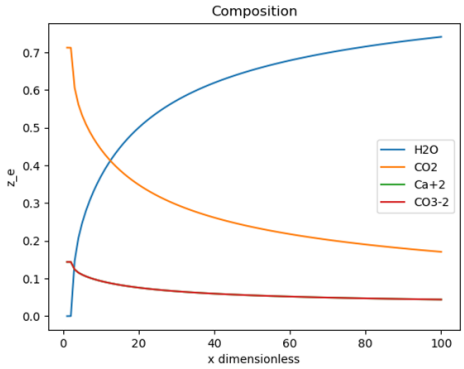

(c) z_e

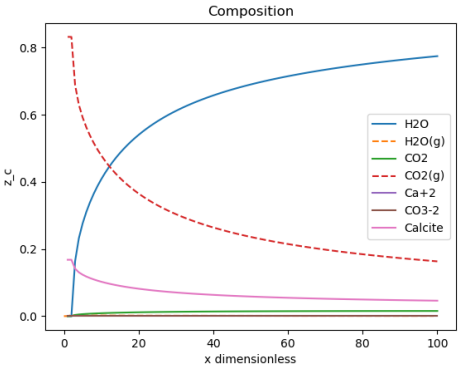

(d) z_c

Figure 4.2: 500 days of injection of CO_2 in 1D reservoir with precipitation of calcite and dry-out

The first cell is dried out after 460 days. At this point in time, only the first cell is completely dried out. In Figure 4.2d, a distinction is made between CO_2 in the gaseous and aqueous phases.

4.3. Porosity treatment

The minerals that are precipitating in the reservoir impact the porosity negatively. In Figure 4.3, the same model is used as in Figure 4.1, where precipitated halite is being dissolved.

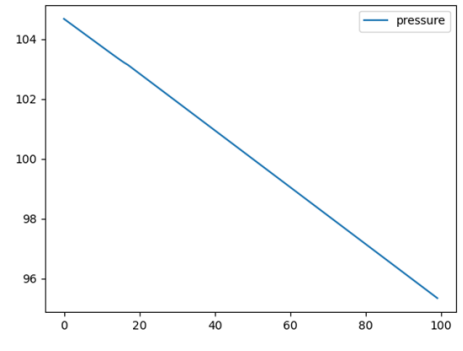

(a) Pressure gradient

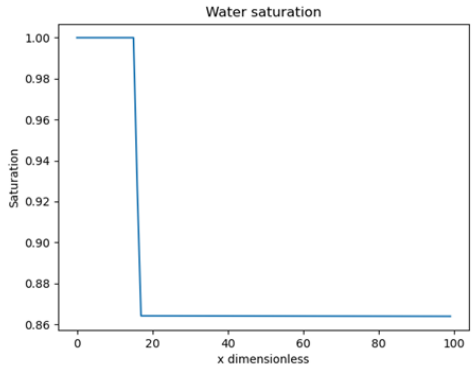

(b) Water saturation of the solution

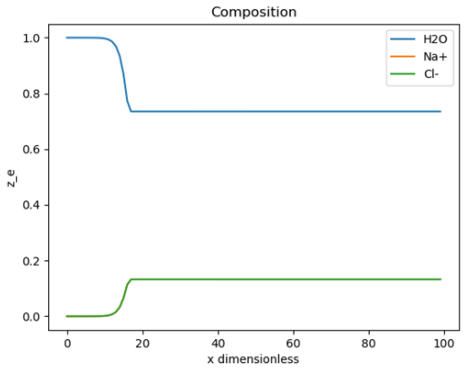

(c) z_e

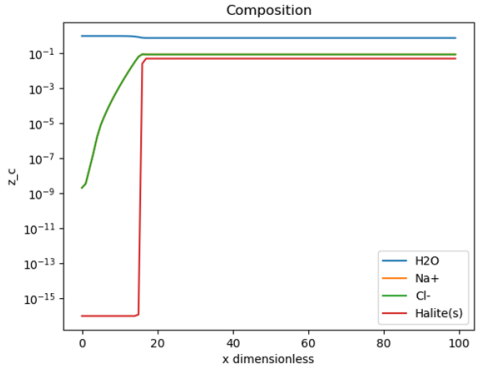

(d) z_c

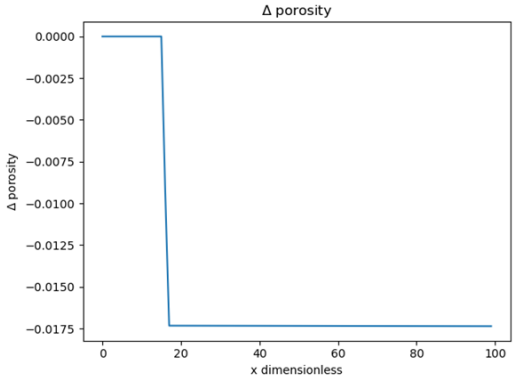

(e) Porosity change

Figure 4.3: 1D dissolution of precipitated salt, injection of pure H_2O in brine with change in porosity

The change in porosity is seen in Figure 4.3e, where the porosity change is relative to the initial porosity. The pure waterfront is located in cell 17, where it has dissolved all of the halite in the cell. The initial condition has a lower porosity, which means less fluid is within the cell. Therefore, the injected water has to push less brine out of the way and is faster. Permeability is not changing, so the fluid is not constrained by rate.

The same porosity treatment can be used on section 4.2, which is shown in Figure 4.4. Here, the same concentrations are used and the same amount of time steps. The only difference is the porosity change.

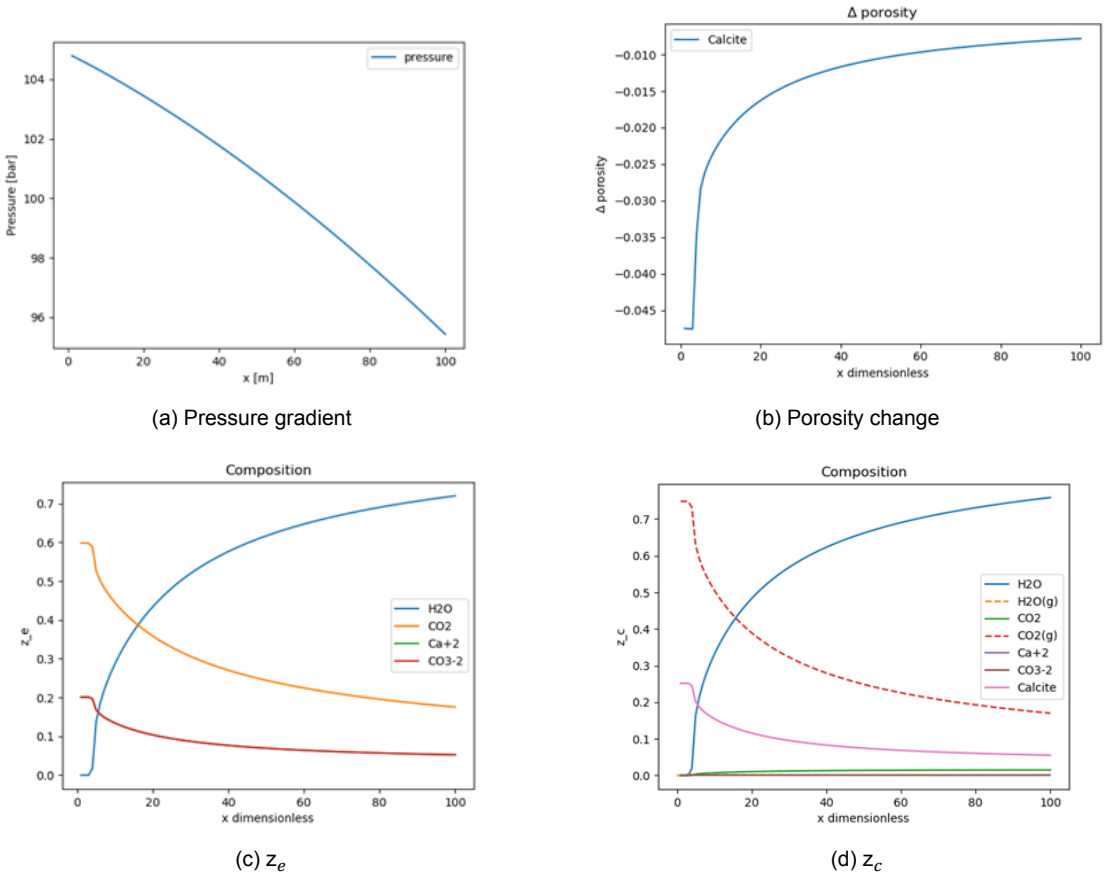

(a) Pressure gradient

(b) Porosity change

(c) z_e

(d) z_c

Figure 4.4: 1D injection of CO_2 in brine with porosity treatment

With this setup, the first three cells are entirely dried out. In the initial condition, the porosity is 0.1989, whereas, in the first cell, the new porosity is 0.153, which is a 23% decrease in porosity due to dry-out.

4.4. Kinetic equilibrium in multiphase flow

All of the previous models have equilibrium reactions. For the next model, the kinetic rate for the equilibrium condition of calcite is calculated. The same parameters and compositions are chosen as in Figure 4.2. Here, the rate is calculated by Equation 2.10, where the rate constant k = 0.1 and the area is calculated according to Equation 2.11.

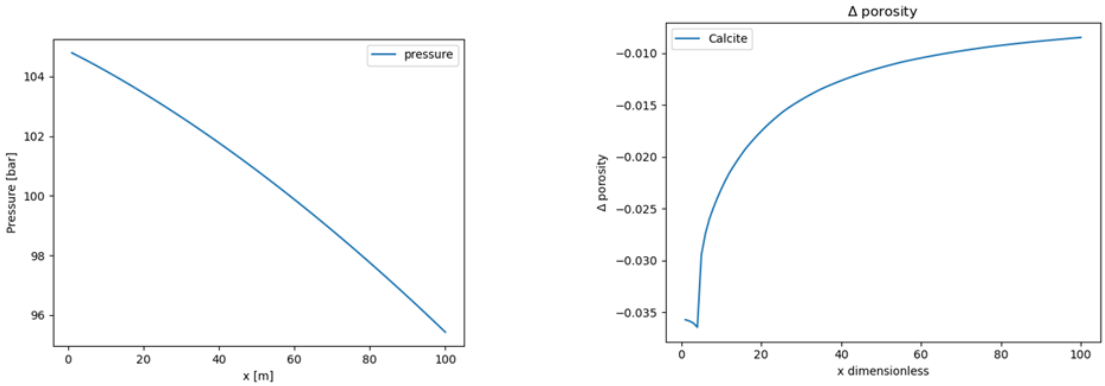

(a) Pressure gradient

(b) Porosity change

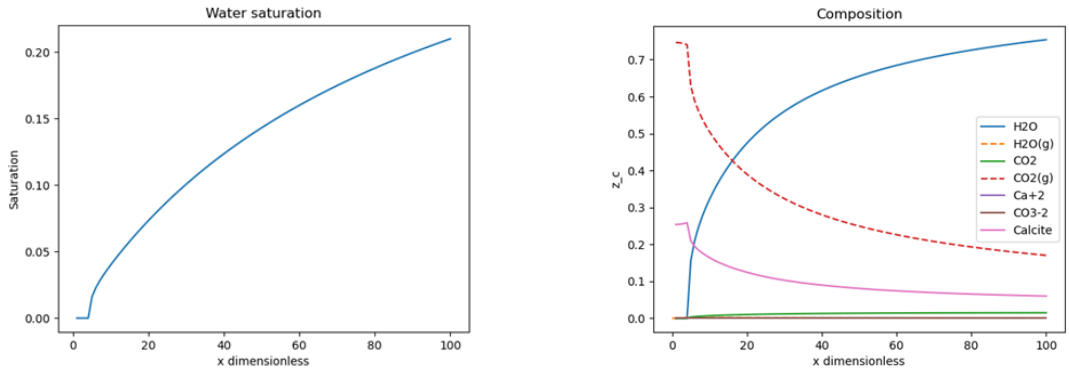

(c) Water saturation

(d) z_c

Figure 4.5: 1D CO_2 injection with kinetic reaction for calcite

The first four cells are entirely dried out. The new porosity of the first cell is 0.165, which is a 17% decrease from the initial condition.

4.5. Benchmark multiphase flow

For the benchmark, a simple multiphase system is chosen with 0.8 M Ca^{+2} and CO_3^{-2}. The cells in the x-dimension will increase in size. The following parameters are used:

Parameter reservoir	Value	PVT	Value
Number of cells	80	Initial pressure	392.517 bar
Cell size	0-24x100x100 m	Inj / prod pressure	492.517 / 382.517 bar
Porosity	0.2	Injection rate	500 m^3/day
Permeability x, y, z	100, 100, 100 mD	Temperature	350 Kelvin
Depth	2000 m	Viscosity fluid / gas	0.45 / 0.0577 cP
Rock compressibility	5.8e^{-7} bar^{-1}	water K_{re} / n	1 / 6
		gas K_{re} / n	0.32 / 2.5

Table 4.2: Reservoir and PVT data used

The injection rate is constrained by BHP, so the rate is constant until this constraint is met.

The viscosity values are an approximation of the values calculated by the EOS of MoReS. The viscosity is constant throughout the DARTS model. The model is run until 10% of the total pore volume is injected, which happens after 400 days. In this benchmark, the Debye-Hückel activity model is used.

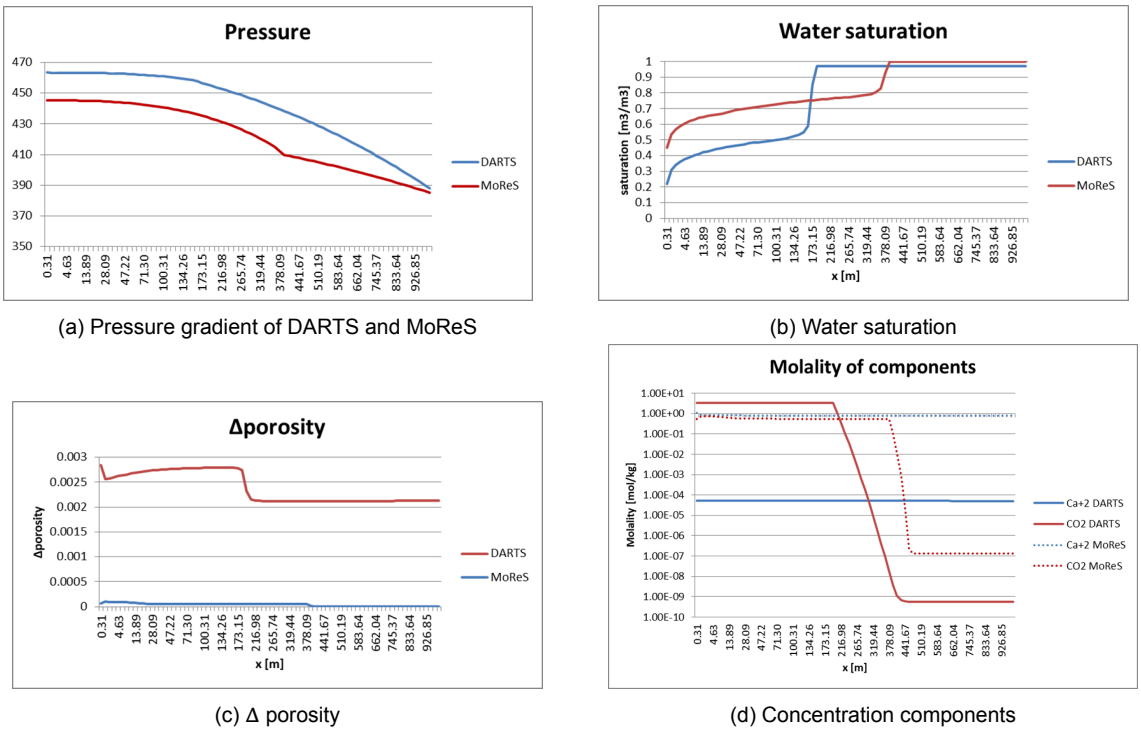

(a) Pressure gradient of DARTS and MoReS

(b) Water saturation

(c) Δ porosity

(d) Concentration components

Figure 4.6: 1D benchmark between DARTS and MoReS for injection of CO_2 into brine

4.6. Single phase pH

For the single-phase buffer reaction, the following reactions are being modeled in a brine:

$$\begin{aligned} OH^- + H^+ &\rightleftharpoons H_2O, \\ CO_3^{-2} + H^+ &\rightleftharpoons HCO_3^-, \end{aligned} \tag{4.2}$$

In this model, H^+ can either form water together with OH^- or form bicarbonate with the buffer CO_3^{-2}. Carbonic acid and the formation of subsequent CO_2 are not modeled in this example, as are any other reactions with the ions (Na^+ and Cl^-) that are present in the brine. This is for simplicity, the pH is the main focus. The initial composition and injection composition is given in Table 4.3. The result of this model is shown in Figure 4.7.

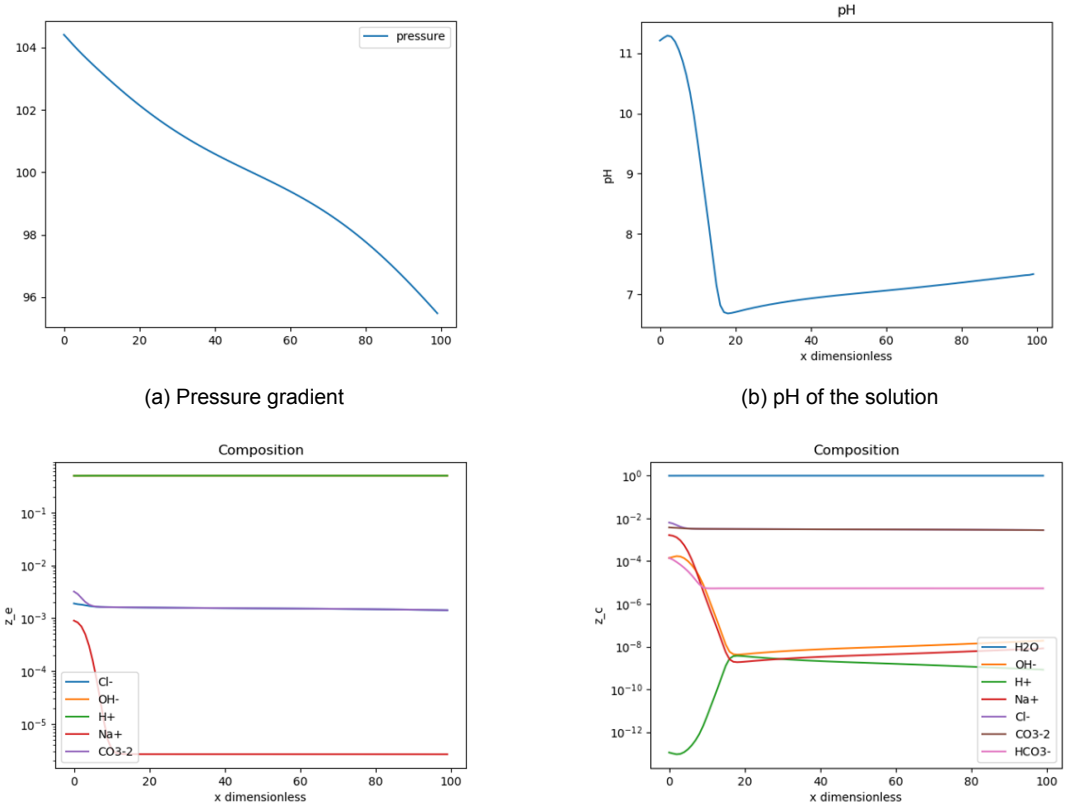

(a) Pressure gradient

(b) pH of the solution

(c) z_e

(d) z_c

Figure 4.7: 1D injection of alkaline water into pH neutral brine

The injected alkaline brine is slowly moving into the neutral brine. This allows for the buffer to react and for the alkaline to slowly dissipate over the entire reservoir. At each time interval, Reaktoro calculates the new pH and the amount of water using the species OH^-, H^+, and $CO3^-2$. As water is a component of the species, it is not being transported by DARTS.

Species	Initial composition	Injection composition
H_2O	1 kg	1 kg
CO_3^{-2}	17.8 mg	5660 mg
Na^+	3931 mg	8270.6 mg
Cl^-	1 mg *	1 mg *

Table 4.3: Concentrations of species in the system. * Concentration is constrained by charge balance

Table 4.1 shows the initial and injection compositions of the brine. The first constraint is pH. For the initial composition, the pH is set to 7 and for the injection composition a pH of 11.1. Reaktoro will calculate how much H^+ is needed to achieve this constraint. In order to still have charge balance, The concentration of Cl^- is determined by the charge balance set to 0.

4.7. Benchmark single phase pH

For the benchmark, a model has been made in MoReS. The injection and initial conditions are the same as Table 4.3. The reservoir and PVT data are as follows:

Parameter reservoir	**Value**	**PVT**	**Value**
Cell size	0.15x5x5 cm	Initial pressure	1 bar
Cells	200	Injection / production pressure	1.2 / 0.95 bar
Porosity	0.2	Injection / production rate	150 / 165 cm^3/day
Permeability	500 mD	Temperature	293 Kelvin
Well radius	0.015cm	Viscosity fluid	1 cP
Rock compr	0 bar^{-1}	K_{re} / n	1 / 2
		Density fluid	1000 kg/m^3
		Fluid compr	0.0001 bar^{-1}

Table 4.4: Reservoir and PVT data used in pH benchmark

The rate is controlled with a pressure constraint for each well. In this example, the injection is chosen so that a single pore volume is injected every day. This simulation is therefore run for half a day, to visualize the front.

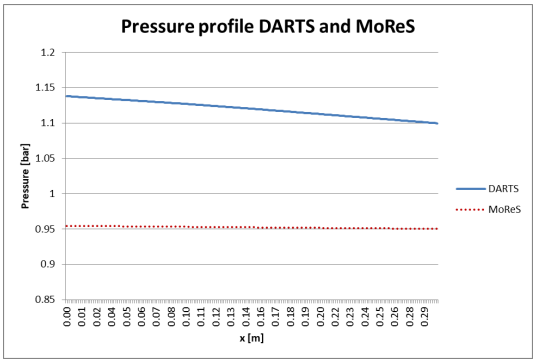

(a) Pressure gradient

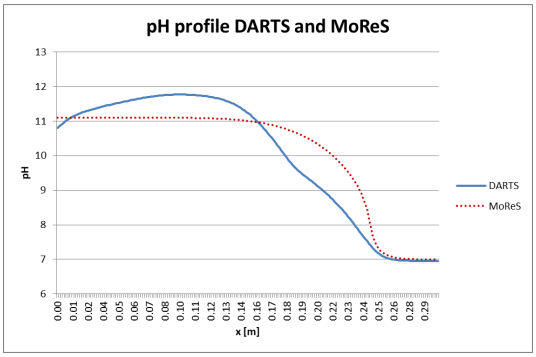

(b) pH of the solution

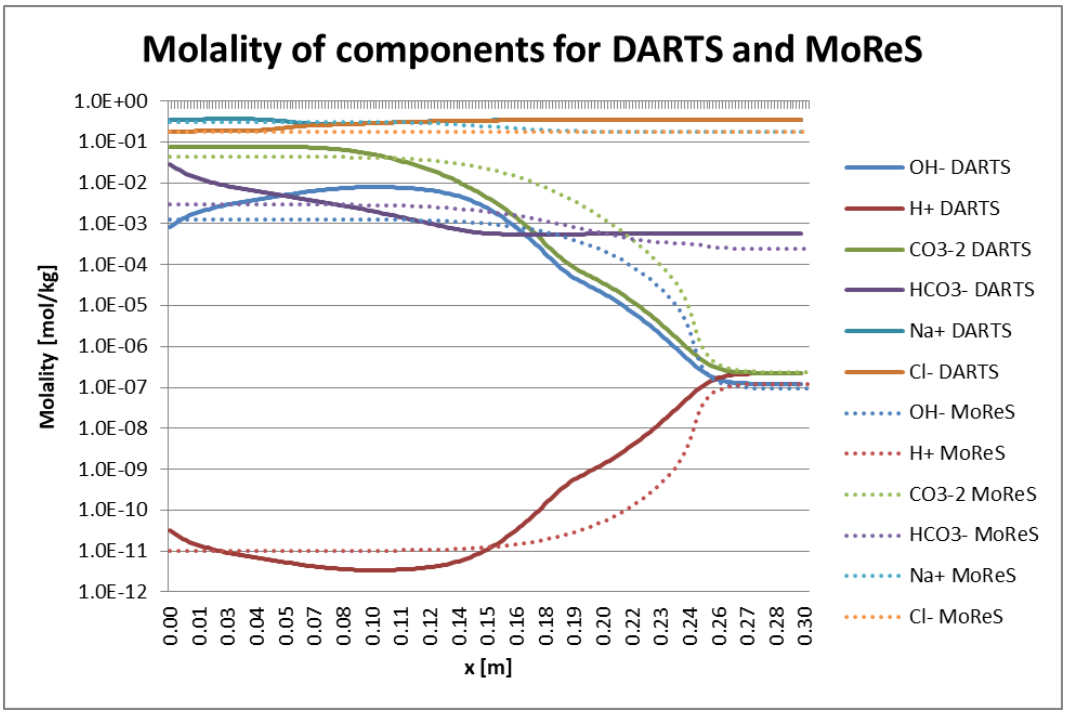

(c) Molality of the components

Figure 4.8: Benchmark between DARTS and MoReS for injection of alkaline brine

The output of MoReS is in molality. The assumption is made that the molar fraction output of DARTS contains one mole. Using the mass of the solvent, the molality can be calculated.

4.8. CO_2 injection into 2D core

In this section, we present a synthetic model of a sandstone core with a small variation of porosity and permeability due to the heterogeneity of the rock. In the core, there are 9 molal of Na^+ and Cl^- each, and 0.8 molal of Ca^{+2} and CO_3^{-2} each present initially. These ions are allowed to precipitate and form solids. The result after 2000 days is shown in Figure 4.9.

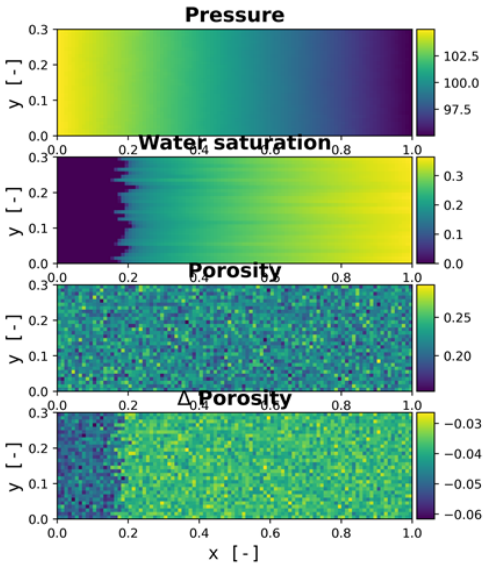

(a) Pressure, saturation, porosity and Δ porosity

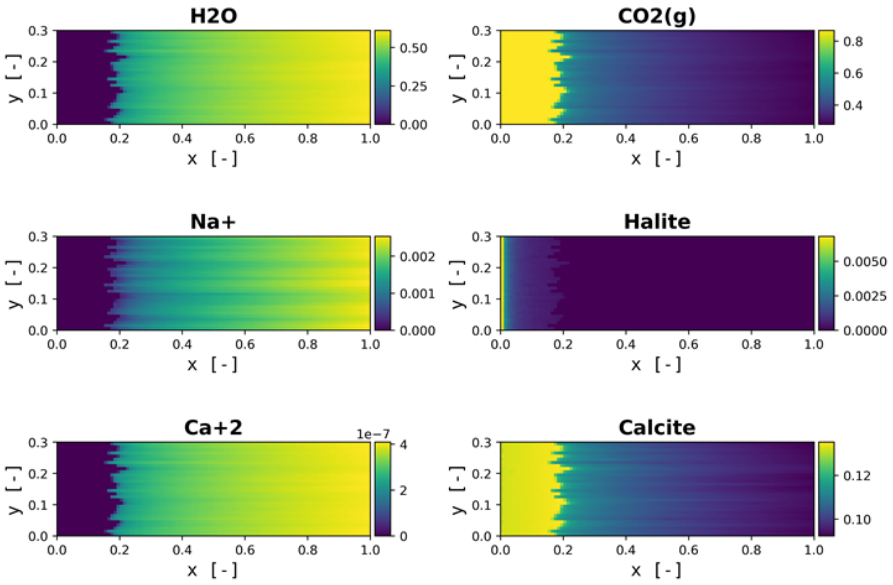

(b) Molar fraction composition

Figure 4.9: 2D injection of CO_2 with precipitation of halite and calcite

Here, the porosity is decreasing near the injection well, which is situated along the whole y-axis.

5

Discussion

In this Chapter, the results are compared and discussed. Furthermore, an explanation is given on how to solve some of the problems encountered. The limitations of DARTS and Reaktoro are explained in the end.

5.1. Precipitation and dissolution

At first, in Figure 4.1, a single-phase aquifer is modeled. Here, by adding ten molal of Na^+ and Cl^- each, halite is precipitating. Pure water is introduced, which is able to dissolve the solid. The ions of the solid are dissolved into the water until the maximum solubility is met. In Figure 4.1c, the species are shown. From this, the concentration of ions is decreasing as expected. The flash from Reaktoro is shown in Figure 4.1d and it shows the components and the concentration of halite. Here, it is clear that the water dissolves the solid and takes up the ions. There is a small transitional period around cell 17, where there is less halite present than in the initial condition, but not none. As this is an equilibrium reaction, the dissolving of halite happens instantaneously if water is able to dissolve more solids.

In the multiphase reactive flow example, shown in Figure 4.2, the model has been run for 500 days, which is past the initial shock. The focus of this simulation was the formation of calcite during the dry-out process. The first reservoir cell has dried out in this example, leaving only gas and solid phase present. From Figure 4.2c, there is an increase in ion concentration near the injection well. The resulting flash is shown in Figure 4.2d, where this increase in ions translates into the precipitation of calcite. From the initial condition, there is a 10.8 times increase in moles of calcite in the first cell. This increase in solids is due to the vaporization of water, which releases the ions. As more water is vaporized, the solution from other cells might replace this water, introducing more ions into the cell. This creates a positive feedback loop, where more ions are introduced in the cell as it is drying.

5.2. Porosity treatment

Porosity treatment has a significant effect on overall transport. If the precipitants are blocking the pore space, fewer fluid pathways are present. Comparing Figure 4.1 and Figure 4.3, shows that, for an equal amount of time steps, the pure H_2O front is five cells further ahead in the model with porosity treatment. This is a 40% increase, which comes from the reduced volume that the fluid needs to pass through. A reduced volume means it can hold fewer fluids, pushing away the fluid of the next cell faster. Only a small decrease in volume, 8.5% in the case of this example, is causing this effect. This means that a low concentration of precipitants can have a large impact on the porosity inside the reservoir.

In multiphase precipitation, shown in Figure 4.2 and Figure 4.4, porosity treatment will have the same influence. Again, the front has propagated further than without porosity change. It takes 23% longer to achieve the same water saturation without porosity treatment. The concentration of calcite has also increased. At the first cell, there is a 16.7 times larger amount of precipitated moles of calcite present as in the example without porosity treatment. This increase in moles gives a 23% decrease in porosity.

5.3. Kinetics

The results shown in Figure 4.5 show kinetic equilibrium. The precipitation or dissolution rate is calculated using Equation 2.10 since Reaktoro does not have a kinetic equilibrium function as of writing. This rate is calculated using the activities of the ions in both equilibrium and initial conditions, which come from Reaktoro. Reaktoro will equilibrate these two systems and calculate the correct activities. The rate constant can be determined from literature. An infinitely large rate constant means that the reaction will behave according to the equilibrium reaction.

Comparing the equilibrium reaction in Figure 4.2 and Figure 4.4, shows that there is more porosity left in the kinetic run. This holds true, as the equilibrium reaction is the most extreme case. The difference in porosity between these two examples is 0.012, which is 6% of the initial porosity.

The difference in porosity mainly comes from the first few days. Appendix 6.2 shows the molar fractions of components and the porosity change over time for the first reservoir cell. It shows that the kinetic example, Figure 3, has initially no precipitation, whereas, in Figure 2, there are instantaneously some precipitants. This immediate blockage of pore space will have a large impact on fluid flow for the time remaining. Complete dry-out comes at a later stage using the kinetics, as the porosity is higher compared to the equilibrium conditions.

5.4. Inconsistency with multiphase interactions

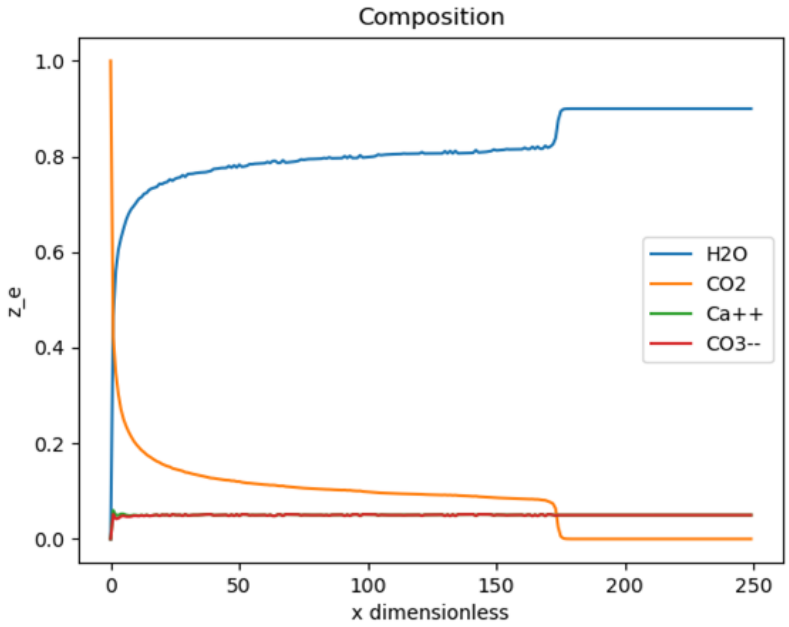

Figure 5.1: Reactive two-phase flow with Calcite formation

In the case of multiphase precipitation, as in section 4.2, the ions are dissolved in the aqueous phase. The model is in two-phase and there is a possibility for the ions to precipitate into calcite. The initial concentrations of the ions are equal, so there is no inconsistency in the charge balance. The result is shown in Figure 5.1. From this figure, it is clear that there is still an inconsistency present, as the molar fractions of H_2O, Ca^{+2}, and CO_3^{-2} are not straight lines. The reason for this inconsistency comes from the way that volume is calculated by Reaktoro, which depends on partial molar volumes. The inconsistency in charge balance is however created by the parametrization method.

5.5. Consequences of precipitants

As modeled, there is a relatively large blockage of pore space, around 17% for a brine. This decrease in porosity will lead to a decrease in permeability, as shown in Equation 1.5. The decrease in porosity and permeability will lead to higher injection pressure to achieve the same throughput of CO_2 gas. The injectivity of the reservoir is severely affected, which can drive up pumping costs and increase the risk of cap rock damage.

If the porosity decreases severely, treatment of the near-wellbore region is needed. In the case of halite and calcite, dissolving is done by injecting pure water to dissolve the precipitants. In the case of calcite, an alkaline solution will also improve the dissolution. The disadvantage is that there is significant downtime and the ions still remain dissolved in the solution. These ions can precipitate again when the injection of gas starts, leading to blockages and again the same treatment.

A water alternating gas (WAG) can be performed to decrease the risk of precipitation, as the water will partially flush the system. However, the total injected volume of gas will be much less than with a continuous injection of CO_2.

5.5.1. Consistency in Reaktoro

The consistency of the properties of Reaktoro has to be tested. For this, ternary phase diagrams can show any inconsistency. In this case, a two-phase system is chosen: a single ion, CO_2, and H_2O. As the concentration of CO_2 increases, the system will go to the gas phase and can hold fewer ions. The ions in the system cannot go to a gaseous or solid phase.

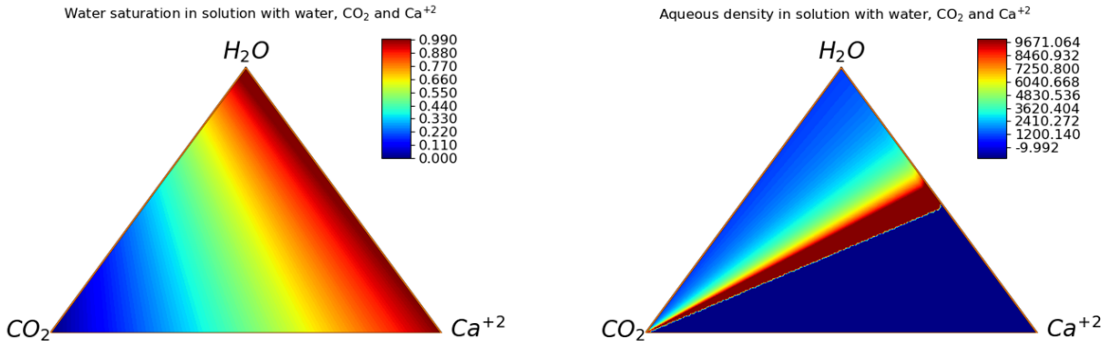

(a) Phase diagram (b) Density diagram

Figure 5.2: Ternary diagram with H_2O, CO_2 and Ca^{+2}

In Figure 5.2, a phase diagram and a density diagram are made for the system. Here, as the amount of Ca^{+2} ions increases relative to the other components, the charge balance is skewed. This results in an unphysical density diagram, where the density goes up and becomes negative in extreme cases. To solve this inconsistency, the system is opened up to a negative ion, such as Cl^-. In doing so, the charge balance will remain 0 for each state of the system. Figure 5.3 shows the properties of the system for all cases with a charge balance of 0.

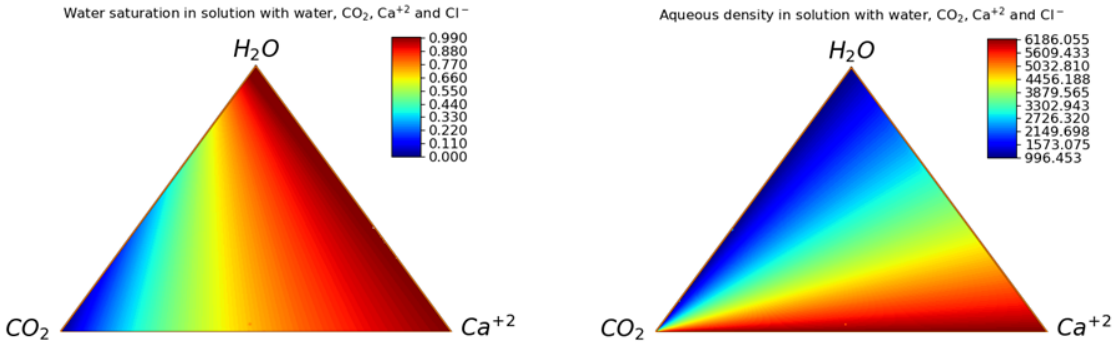

(a) Phase diagram (b) Density diagram

Figure 5.3: Ternary diagram with H_2O, CO_2, and Ca^{+2}, system is set at a charge balance of 0 with Cl^-

The main difference between these two examples is that the addition of Cl^- increases the aqueous phase fraction and increases the aqueous density.

5.5.2. Partial molar volume and OBL

Using partial molar volume values for each component, the volume can be calculated as:

$$V = n \sum x_i \overline{V}_i, \tag{5.1}$$

where $\overline{V}_i$ is the partial mole volume of the component. This equation can be used for both the overall volume and a volume of a single phase. Ions can have negative values, as they interact with the water molecules and disturb their arrangement or they can fit between the water molecules. Using this volume, the density can be computed using the total mass present in the system or per phase. The partial molar volumes come from databases and are a function of pressure and temperature. The partial molar volumes taken by Reaktoro come from a database and Figure 5.4 show the values of the PHREEQC database for Na^+ and Cl^-.

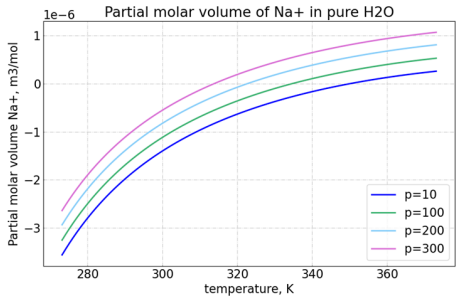

(a) Partial molar volume values for Na^+ ion

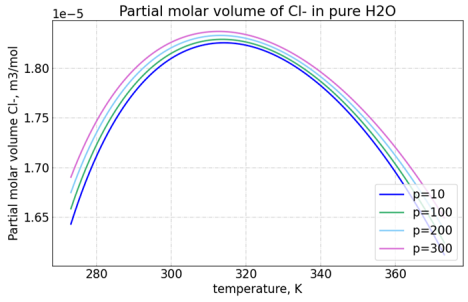

(b) Partial molar volume values for Cl^- ion

Figure 5.4: Partial molar volumes in pure H_2O

The values of partial molar volume only depend on the temperature and pressure in the system, whereas composition is not taken into account inside the databases. Therefore, it is possible for a state to have negative volume. For the creation of a cube in OBL, the vertices vary in concentration. A schematic of this OBL method is given in Figure 5.5, which shows a single cube with varying concentrations of ions.

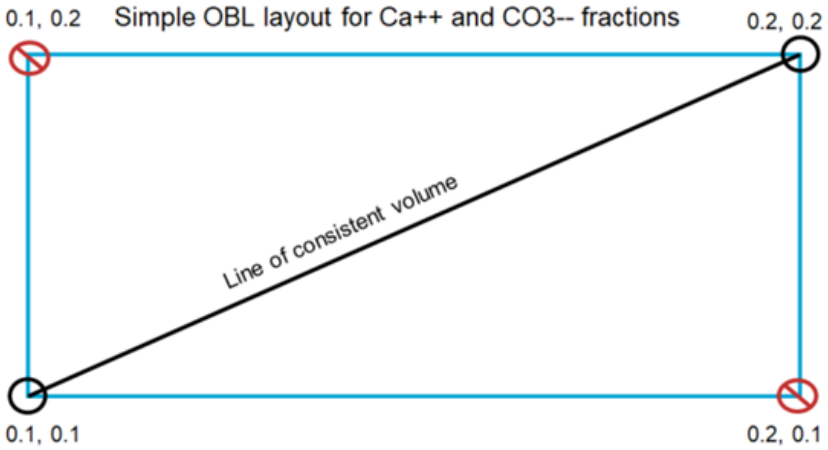

Figure 5.5: Consistency when applying OBL

Here, OBL calculates the properties at the vertices of the grid block. The problem is that, at two vertices of the grid block, the ions are not in balance. This imbalance gives a large difference in properties, among which is the volume. The volume at the imbalanced vertices has a possibility to be negative and this creates highly variable solutions within the cube. Therefore, these imbalanced vertices must not be taken into account when applying OBL. Taking these inconsistent vertices out, a plane is projected of consistent properties. This plane is where the properties are consistent as the ions are balanced.

5.6. pH reactions

Reactions that influence the pH are very common in the reservoir, especially with the introduction of CO_2. Dissolved CO_2, which was present in the multiphase results, shown in Figure 4.2, can react with water to form carbonic acid. This acid can then release H^+ into the aqueous solution, decreasing the pH. This is not modeled in Figure 4.7 but gives a good basis to start modeling complex systems.

In Figure 5.6b, the pH is plotted in the reservoir. Due to the implicit method, there is some smearing present, which causes a small inaccuracy at the front. This error can be minimized by increasing the resolution of the reservoir or decreasing the time steps.

The initial composition of the brine is found in Table 4.3, where there is a charge balance and a pH constraint set. Therefore, the exact concentrations are calculated by Reaktoro. The buffer immediately reacts with the brine present and forms HCO_3^-, increasing the pH. The larger the concentration of CO_3^{-2} is, the more H^+ can react and the higher the pH is. As more H^+ reacts, the equilibrium between H^- and OH^- will also shift, causing more OH^- to be free in the brine. This also means that less water is present, but these are small amounts in the range of $1e^{-4}$.

5.6.1. Resolution for low concentrations

The parameterization method can also have issues with resolution, when the concentrations at the vertices differ too much, the reaction can not be interpolated. In the case of section 4.6,

the pH change has a high sensitivity. A small change in concentration of H^+ gives a large change in pH as shown in:

$$pH = -log[H^+], \tag{5.2}$$

and it shows that there is a logarithmic relationship between the concentration of H^+ and the pH. A small model is built with ten cells and with the system described in Equation 4.2. If the resolution used is 101 points for each species, there is a difference of $1e^{-2}$ between each vertex of a hypercube. Within this difference, the reaction should behave as linearly as possible to get the best value for interpolation. If there is non-linear behavior within this cube, the interpolation result will have an error. This error can be seen in Figure 5.6. In this figure, the initial state of the system is in equilibrium at a pH of 7 and a buffer solution is injected with a pH of 11.

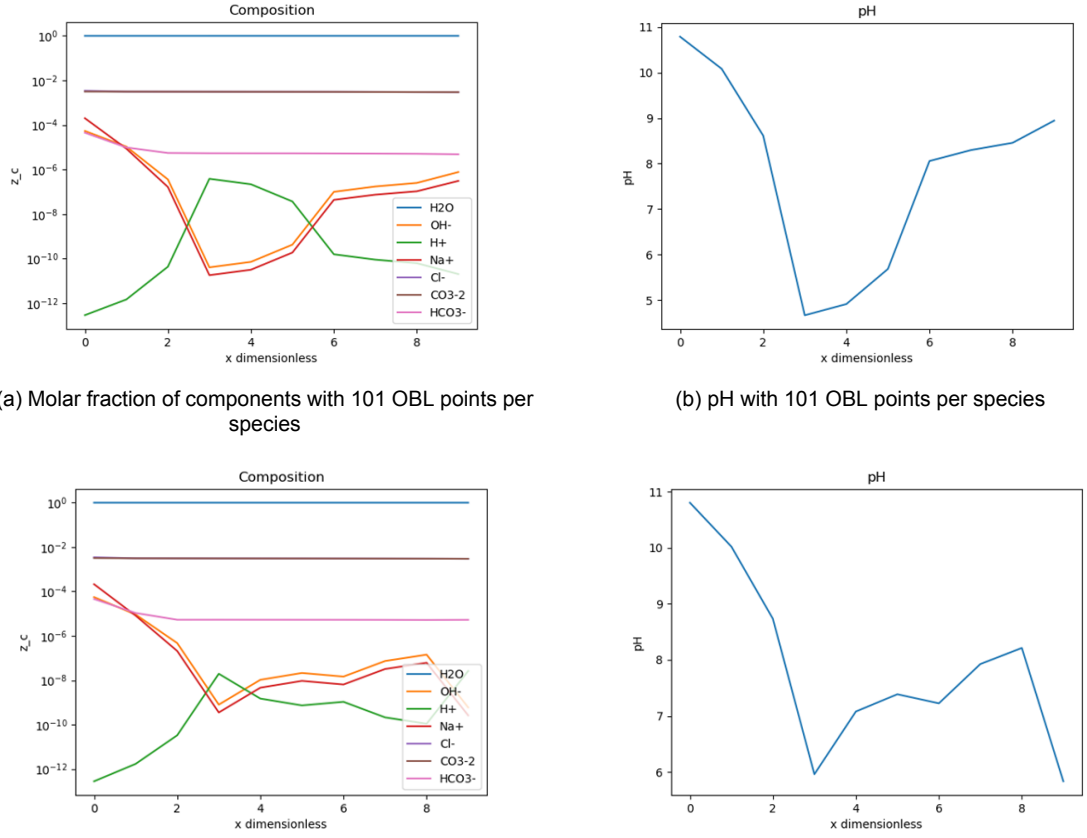

(a) Molar fraction of components with 101 OBL points per species

(b) pH with 101 OBL points per species

(c) Molar fraction of components with 1001 OBL points per species

(d) pH with 1001 OBL points per species

Figure 5.6: Solution with initial pH of 7 and injection of 11 with CO_3^{-2} acting as a buffer with a difference in OBL resolution

As shown, the pH will decrease to 5, which is not a correct chemical solution. There is a dip in the concentration of the buffer shown between cells 3 and 5, which is inconsistent. In the same system, the resolution is increased to 1001 points for each species, as shown in Figure 5.6cd. Here, the inconsistency is much smaller, but still there. This means that when the OBL resolution is increased, the error will decrease. The disadvantage is that more cubes need to be created for each run, making it more computationally expensive.

In order to check the nonlinearity of the solution, the species composition of extremes is taken.

This means that the composition that results in a pH of 5 and pH of 11 is taken to check what happens in between. The values between these points are taken linearly in standalone Reaktoro to avoid the influence of DARTS. The result is shown in Figure 5.7.

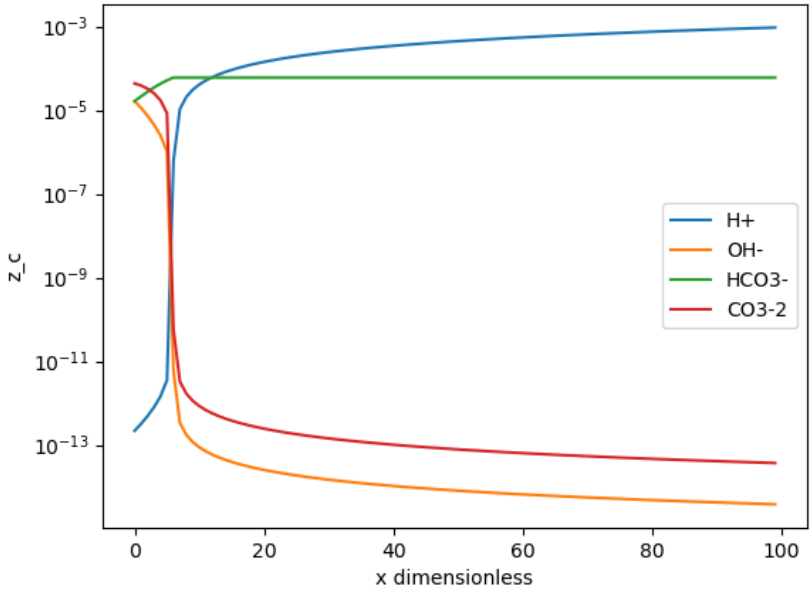

Figure 5.7: Linear input between pH extremes of Figure 5.6a inside standalone Reaktoro

As expected, the system is very sensitive to small increases in H^+ concentration. If a vertex of a cube has such a concentration of H^+ that the buffer has reacted fully, the pH will increase significantly. In order to capture this non-linear relationship, the resolution must be increased until it becomes a linear relationship. If the difference between vertices is small enough, the interpolation result will be consistent. The downside is that more vertices need to be calculated.

Next, increasing the points per species has an upper limit. For a 64-bit computer, the maximum storage of an array is 2^{64}-1. That means, for our system, outlined in Equation 4.2, there are 5 species, so the maximum amount of points will be:

$$\sqrt[5]{(2^{64}-1)} \approx 7131, \tag{5.3}$$

which will give us a resolution of 0.00014, which is still too large to capture the reaction accurately, as the concentration of H^+ is around $1e^{-13}$ mole.

Therefore, instead of taking each species from 0 to 1, the boundary can be set more strictly. For the upper bound, for example:

$$max(z_{inj}, z_{ini}) + |z_{inj} - z_{ini}|, \tag{5.4}$$

if the absolute difference is larger than the maximum vertex difference. If the next vertex is further than this difference, the solution needs to be extrapolated, bringing error into the system. However, bounding this maximum and minimum value for each individual species

will still bring an error into the system. Therefore, the sensitivity of the individual species needs to be analyzed.

Since the pH is very sensitive, every species that does not play a role can be set to a low number of points for the formation of OBL points. In this case, the species Na^+ and Cl^- do not interact with H^+ and do not need to have a high resolution. The species CO_3^{-2} and OH^- on the other hand, do play a role. They are connected to the pH due to the reactions: CO_3^{-2} interacts to form HCO_3^- and OH^- to form H_2O. Therefore, it can be decided that Na^+ and the pressure will only have a resolution of 101 points, which leaves more space for the sensitive species. In this case, the species that regulate the pH can be set to 100001 points.

With these steps, the resolution can be improved such that the result is physical, which is shown in Figure 4.7.

5.7. Benchmark

The benchmark has been performed against MoReS, the geochemical simulator from Shell. Using the same inputs, a multiphase system and a pH system have been modeled. Due to time constraints, the best-fitting match is presented in this work.

5.7.1. Multiphase benchmark

In the multiphase benchmark, shown in Figure 4.6, there are many differences. At first, the EOS viscosity model is not implemented in DARTS, so a constant viscosity is used. The pressure is much higher in the DARTS model and the shock is not as visible as in MoReS. The same quantity of gas is injected into the system, but in DARTS, the front has not passed as far as in MoReS. This leads to quicker dry-out. The phase densities calculated by MoReS vary by roughly 20% from the phase densities calculated by Reaktoro using the same database and activity model. The reason could be that MoReS injects the CO_2 at 293 Kelvin. The molality of the ions is much higher in the aqueous phase with MoReS, which leads to less formation of calcite and therefore a smaller difference in porosity. Almost all of the ions in DARTS are precipitated. This leads to a difference in porosity of 29 times larger.

5.7.2. pH benchmark

The pH benchmark, shown in Figure 4.8, shows that there is a large pressure difference between the two models. The pressure profile of DARTS is much higher than the pressure profile of MoReS. In DARTS, the pressure is building up, whereas in MoReS, a connection between the wells is quickly established and the production well determines the overall pressure in the core.

For the pH, DARTS has more numerical dispersion than MoReS. The pH concentration does not have a sharp front and is smeared over a longer area of the core. Moreover, the injection pH is set at 11.1, as described in Table 4.3, but in the results, the maximum pH is 11.78. This can be due to numerical dispersion, but could also be due to how the maximum and minimum concentrations are set. As described in section 5.6, the resolution of OBL and the concentration boundaries set have a large influence on the resulting pH. The initial pH is accurate at

7.

Finally, the concentration of components in molal. As it is an alkaline injection, the concentration of H^+ is around $1e^{-11}$ molal and will go to $1e^{-7}$ molal at neutral pH. The opposite is true for OH^-, which has an injection concentration of $1e^{-3}$. The concentration of CO_3^{-2} and HCO_3^- is the most important reaction for this problem. Even as DARTS does not completely reflect the MoReS solution, it is fairly accurate given the much higher dispersion.

5.8. Limitations of DARTS and Reaktoro

5.8.1. DARTS

DARTS has the advantage of using OBL, as it is computationally inexpensive and easy to set up, but this method also comes with disadvantages. The main limitation that the OBL approach has, is that for sensitive reactions, such as pH change, the shift in concentrations of the vertices calculated is too large. This is described in section 5.6. It means that the interpolation between vertices is nonlinear and can give nonphysical results. The resolution of OBL can be increased but comes at a computational cost.

5.8.2. Reaktoro

For this work, Reaktoro version 2 is chosen, which is an improvement over version 1. However, as of writing this, Reaktoro version 2 is not yet fully complete. There are missing components such as surface adsorption and kinetic equilibrium calculations. As the kinetics could be replaced by a kinetic rate equation, which is shown in Equation 2.10, surface adsorption cannot.

During simulations, Reaktoro has the possibility of on-demand machine learning and is using the python package Optima for solving linear and non-linear optimization problems. At some intervals, optima calculation cannot succeed, which results in an equilibrium calculation that is not at the minimum Gibbs energy. Rerunning the input of this failed optima calculation in a fresh stand-alone Reaktoro can result in finding correctly equilibrated results again. The difference between the compositions of these runs is roughly relatively small, in the order of 10^-2 but can be a source/sink for the mass balance. Most of these sub-optimal equilibrium calculations are at phase transition boundaries. At these points, Reaktoro has issues calculating the minimal Gibbs energy. The effect is exacerbated when non-ideal activity models are used, due to the increased complexity.

An example is shown in Figure 5.8, where Reaktoro is unable to find the correct solution at the phase transition boundary.

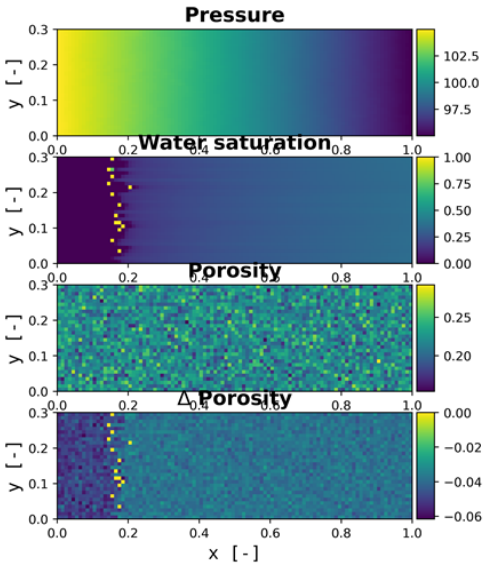

(a) Pressure, saturation, porosity and Δ porosity

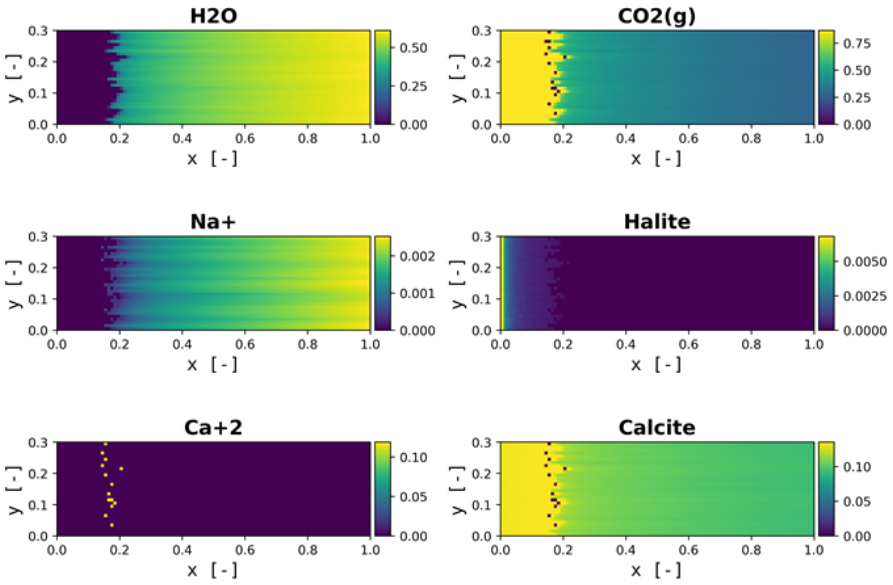

(b) Molar fraction composition

Figure 5.8: 2D injection of CO_2 without correction for Reaktoro

This result is the same as in Figure 4.9, but Reaktoro is not corrected. This results in some points at the phase interchange that are outliers. These points have not been equilibrated correctly. In these cases, Reaktoro flips between two cases, one without accurate equilibrium and one close. Depending on the maximum iterations, there is a chance that the non-equilibrated state is used. This results in wrong saturations and reactions, which can be seen throughout the core.

An ionic exchange model has been attempted but was unable to work. The ionic exchange species do not have any properties, so calculating the density of the entire system was not

possible. This meant that Na^+ did partake in the system, but NaX did not. Using the approach as set in subsection 5.6.1 could resolve the issue.

5.8.3. Coupling assumptions and limitations

Whilst coupling, some assumptions have to be made. For instance, DARTS uses molar fractions inside the transport computations. As Reaktoro cannot handle this input, it is assumed that every calculation has exactly one mole, making the fractions into moles.

Furthermore, in the case of halite precipitation, there is an overall loss in precipitants. As shown in Figure 5.9, 10 M of Na^+ and Cl^- ions are added into the system, forming a baseline of precipitants. At the CO_2 front, this concentration of precipitants declines, which is shown as an increase in porosity. When a control volume is completely dried out, there is a slight decrease in porosity, but nowhere near the baseline. Contradictory, calcite precipitation is as expected. In this example, 0.8 M of Ca^{+2} and CO_3^{-2} has been added to the system, allowing precipitation. The total decrease in porosity is mostly caused by calcite.

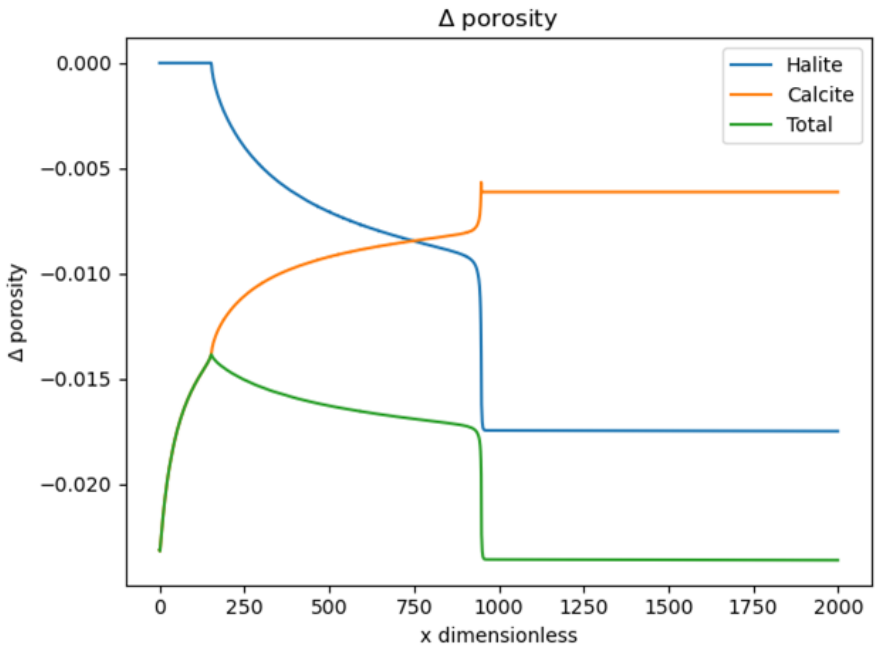

Figure 5.9: Porosity change due to dry out with two minerals

The reason for this removal of precipitants is unknown. The solubility of Na^+ and Cl^- ions does not increase when CO_2 is also dissolved in the solution.

6

Conclusions and Recommendations

6.1. Conclusions

In this thesis, a framework for fully implicit multiphase reactive transport has been built using DARTS and the geochemical package Reaktoro. This framework applies the Operator-Based Linearization (OBL) approach together with a Gibbs Energy Minimization (GEM) scheme to model reactive transport and flow. This solver can be applied to a multitude of chemical reactions inside reservoirs.

It was determined that component- to species-based transport is a numerically stable approach to the flow and transport of components. The component-based equations are reduced to species-based mass balance equations. This allows for the coupling of the geochemical reactions.

The equilibrium calculation and flash are done by Reaktoro using the PHREEQC database and an activity model. Reaktoro determines the distribution of components across phases, which DARTS is able to use for the transport and flow equations. Within a single time step, the control volume has been equilibrated and subsequently transported. This makes the solver flexible and able to handle large time steps, but computationally more expensive.

One such application modeled in this thesis is when gaseous CO_2 is injected into an aquifer for storage. The gas not only displaces the brine but also vaporizes the water. This leads to the dry-out effect, in which ions dissolved in the water, are able to precipitate. Using porosity treatment, 23% of the porosity of the first cell is occupied by calcite if the initial condition is 8 molal ions each. The precipitation of ions can be modeled using equilibrium reactions by Reaktoro or kinetic equilibrium reactions using a kinetic rate. Using the kinetic equilibrium for the same system, the porosity is decreased by 17%.

Another application is the injection of an alkaline solution into a neutral aquifer. A buffer is injected into the aquifer to increase the pH. This buffer and the reactions are modeled throughout the reservoir.

The benchmark shows that there are some small discrepancies between the two simulators, which are mainly due to numerical dispersion or physics that are not added to the DARTS

model. Due to time constraints, the best-fitting solution has been used.

The limitation of DARTS is the resolution of the OBL approach. Sensitive reactions, such as pH, have small room for error. Using a variable resolution for each species, depending on their importance to the reaction, the number of points inside of the parameter space is changed. The boundaries can be adapted to suit the problem more, improving resolution. This method is computationally more expensive, however, the results are physical.

Furthermore, due to the parameterization calculation, there is a discrepancy in the charge balance. This results in nonphysical properties being calculated by Reaktoro. A plane of consistency can be projected in the hypercube that will allow for charge balance along the plane.

The main limitation for Reaktoro is that version 2 is not yet fully implemented. There is no kinetics and surface adsorption. Furthermore, at the phase transition boundary, Reaktoro will have issues calculating the correct equilibrium. This can result in wrong saturations, which can impact the run negatively.

All in all, we have modeled and quantified the porosity change inside the reservoir when injecting dry CO_2. The dry-out effect has been observed. Reaktoro is able to perform the equilibration of the system with and the distribution of phases. Furthermore, a simple pH problem has been introduced to OBL, which can be elaborated upon to be included in the CO_2 injection.

6.2. Recommendations

Several items that are not touched on in this thesis were either not feasible due to time constraints or version compatibility. At first, Reaktoro version 2 has not released the full capacities yet, which does not allow us to do some of the reactions accurately. The implementations that are needed to reach a fully coupled system that can handle all of the necessary reactions would include the following:

- Kinetic rate
- Surface adsorption

The kinetic rate has been estimated using equations, but these require input from the user and can be inaccurate. Furthermore, surface adsorption is an important process in oil extraction, but is not able to be implemented yet.

Due to time constraints, more complicated systems were not investigated. With CO_2 injection, the resulting solution can become acidic, due to the formation of carbonic acid. This process has not been modeled, but is essential, especially in brine prone to calcite formation.

The results of this framework can be validated by core experiments, such as Sokama-Neuyam, Ursin, and Boakye (2019) or using an analytical model. With an extension of the physics, as proposed, a detailed analysis of experiments can improve the validity of the models.

References

Beck, M., Rinaldi, A. P., Flemisch, B., & Class, H. (2020). Accuracy of fully coupled and sequential approaches for modeling hydro- and geomechanical processes. *Computational Geosciences*, *24*(4), 1707–1723. doi: 10.1007/s10596-020-09987-w

Bradshaw, J., Bachu, S., Bonijoly, D., Burruss, R., Holloway, S., Christensen, N. P., & Mathiassen, O. M. (2007). Co2 storage capacity estimation: Issues and development of standards. *International Journal of Greenhouse Gas Control*, *1*(1), 62–68. doi: 10.1016/s1750-5836(07)00027-8

Gunter, W. D., Perkins, E. H., & McCann, T. J. (1993). Aquifer disposal of co2-rich gases: Reaction design for added capacity. *Energy Conversion and Management*, *34*(9-11), 941–948. doi: 10.1016/0196-8904(93)90040-h

Karpov, I. K., Chudnenko, K. V., & Kulik, D. A. (1997). Modeling chemical mass transfer in geochemical processes; thermodynamic relations, conditions of equilibria and numerical algorithms. *American Journal of Science*, *297*(8), 767–806. doi: 10.2475/ajs.297.8.767

Khait, M., & Voskov, D. (2018). Adaptive parameterization for solving of thermal/compositional nonlinear flow and transport with buoyancy. *SPE Journal*, *23*(02), 522–534. doi: 10 .2118/182685-pa

Knodel, M. M., Kräutle, S., & Knabner, P. (2022). Global implicit solver for multiphase multicomponent flow in porous media with multiple gas components and general reactions. *Computational Geosciences*, *26*(3), 697–724. doi: 10.1007/s10596-022-10140-y

Kosakowski, G., & Watanabe, N. (2014). Opengeosys-gem: A numerical tool for calculating geochemical and porosity changes in saturated and partially saturated media. *Physics and Chemistry of the Earth, Parts A/B/C*, *70-71*, 138–149. doi: 10.1016/j.pce.2013.11 .008

Kulik, D. A., Wagner, T., Dmytrieva, S. V., Kosakowski, G., Hingerl, F. F., Chudnenko, K. V., & Berner, U. R. (2012). Gem-selektor geochemical modeling package: Revised algorithm and gems3k numerical kernel for coupled simulation codes. *Computational Geosciences*. doi: 10.1007/s10596-012-9310-6

Lavrov, A. (2016). Dynamics of stresses and fractures in reservoir and cap rock under production and injection. *Energy Procedia*, *86*, 381–390. doi: 10.1016/j.egypro.2016.01.039

Leal, A. M., Kulik, D. A., & Kosakowski, G. (2016). Computational methods for reactive transport modeling: A gibbs energy minimization approach for multiphase equilibrium calculations. *Advances in Water Resources*, *88*, 231–240. doi: 10.1016/j.advwatres .2015.11.021

Leal, A. M., Kulik, D. A., & Saar, M. O. (2016). Enabling gibbs energy minimization algorithms to use equilibrium constants of reactions in multiphase equilibrium calculations. *Chemical Geology*, *437*, 170–181. doi: 10.1016/j.chemgeo.2016.05.029

Lichtner, P. C. (1985). Continuum model for simultaneous chemical reactions and mass transport in hydrothermal systems. *Geochimica et Cosmochimica Acta*, *49*(3), 779–800. doi: 10.1016/0016-7037(85)90172-3

Margert, A., & Voskov, D. (2019). Dissolution patterns prediction in carbonate system.

Masson-Delmotte, Zhai, V., Pörtner, H.-O., Roberts, D., Skea, J., Shukla, P., … (eds.), T. W. (2018). Global warming of 1.5°c. an ipcc special report on the impacts of global warming

of 1.5°c above pre-industrial levels and related global greenhouse gas emission pathways, in the context of strengthening the global response to the threat of climate change, sustainable development, and efforts to eradicate poverty. *Cambridge University Press*, 3-24. doi: 10.1017/9781009157940.001.

Molins, S., Carrera, J., Ayora, C., & Saaltink, M. W. (2004). A formulation for decoupling components in reactive transport problems. *Water Resources Research*, *40*(10). doi: 10.1029/2003wr002970

Parkhurst, D. L., & Appelo, C. (2013). Description of input and examples for phreeqc version 3: A computer program for speciation, batch-reaction, one-dimensional transport, and inverse geochemical calculations. *Techniques and Methods*. doi: 10.3133/tm6a43

Peysson, Y., André, L., & Azaroual, M. (2014). Well injectivity during co2 storage operations in deep saline aquifers—part 1: Experimental investigation of drying effects, salt precipitation and capillary forces. *International Journal of Greenhouse Gas Control*, *22*, 291–300. doi: 10.1016/j.ijggc.2013.10.031

Pörtner, H.-O., Roberts, D., Tignor, M., Poloczanska, E., Mintenbeck, K., Alegría, A., … (eds.), B. R. (2022). Climate change 2022: Impacts, adaptation, and vulnerability. contribution of working group ii to the sixth assessment report of the intergovernmental panel on climate change. *Cambridge University Press*.

Roels, S. M., El Chatib, N., Nicolaides, C., & Zitha, P. L. (2016). Capillary-driven transport of dissolved salt to the drying zone during CO_2 injection in homogeneous and layered porous media. *Transport in Porous Media*, *111*(2), 411–424. doi: 10.1007/s11242-015-0601-y

Sokama-Neuyam, Y. A., Ursin, J. R., & Boakye, P. (2019). Experimental investigation of the mechanisms of salt precipitation during co2 injection in sandstone. *C*, *5*(1), 4. doi: 10.3390/c5010004

Steefel, C. I., & MacQuarrie, K. T. (1996). Approaches to modeling of reactive transport in porous media. *Reactive Transport in Porous Media*, 83–130. doi: 10.1515/9781501509797-005

Valocchi, A. J., & Malmstead, M. (1992). Accuracy of operator splitting for advection-dispersion-reaction problems. *Water Resources Research*, *28*(5), 1471–1476. doi: 10.1029/92wr00423

Voskov, D. V. (2017). Operator-based linearization approach for modeling of multiphase multi-component flow in porous media. *Journal of Computational Physics*, *337*, 275–288. doi: 10.1016/j.jcp.2017.02.041

Xu, T., Sonnenthal, E., Spycher, N., & Pruess, K. (2006). Toughreact—a simulation program for non-isothermal multiphase reactive geochemical transport in variably saturated geologic media: Applications to geothermal injectivity and co2 geological sequestration. *Computers and Geosciences*, *32*(2), 145–165. doi: 10.1016/j.cageo.2005.06.014

Yeh, G.-T., & Tripathi, V. S. (1991). A model for simulating transport of reactive multispecies components: Model development and demonstration. *Water Resources Research*, *27*(12), 3075–3094. doi: 10.1029/91wr02028

Appendices

Appendix I:

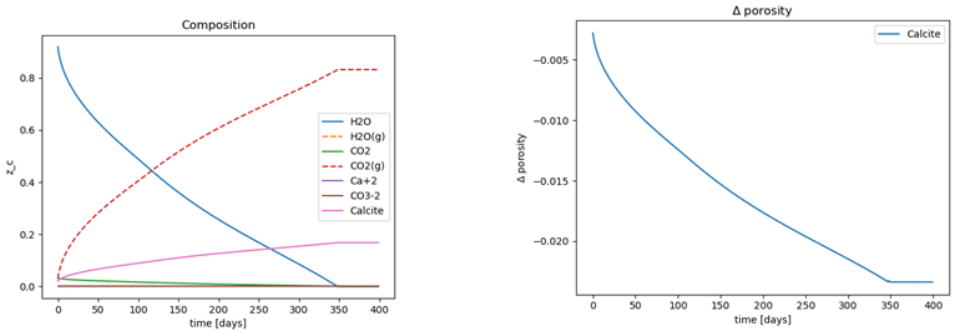

(a) Change in z_c over time (b) Porosity change over time

Figure 1: Change over time for the first cell, with no porosity treatment

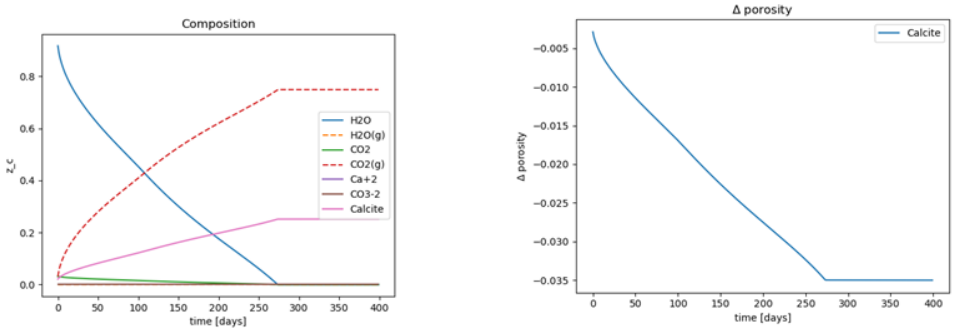

(a) Change in z_c over time (b) Porosity change over time

Figure 2: Change over time for the first cell with porosity treatment

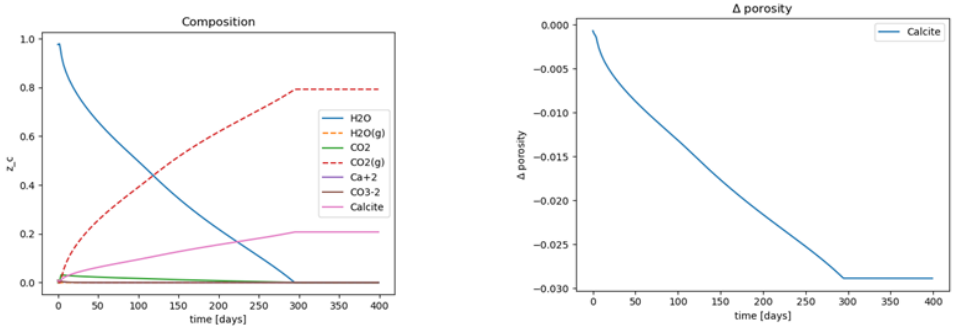

(a) Change in z_c over time (b) Porosity change over time

Figure 3: Change over time for the first cell, with kinetic equilibrium, k = 0.05